UCRL-52265

AN INVESTIGATION OF PRESSURE TRANSIENT PROPAGATION IN PRESSURIZED WATER REACTOR FEEDWATER LINES

S. B. Sutton

July 22, 1977

Prepared for U.S. Energy Research & Development Administration under contract No. W-7405-Eng-48

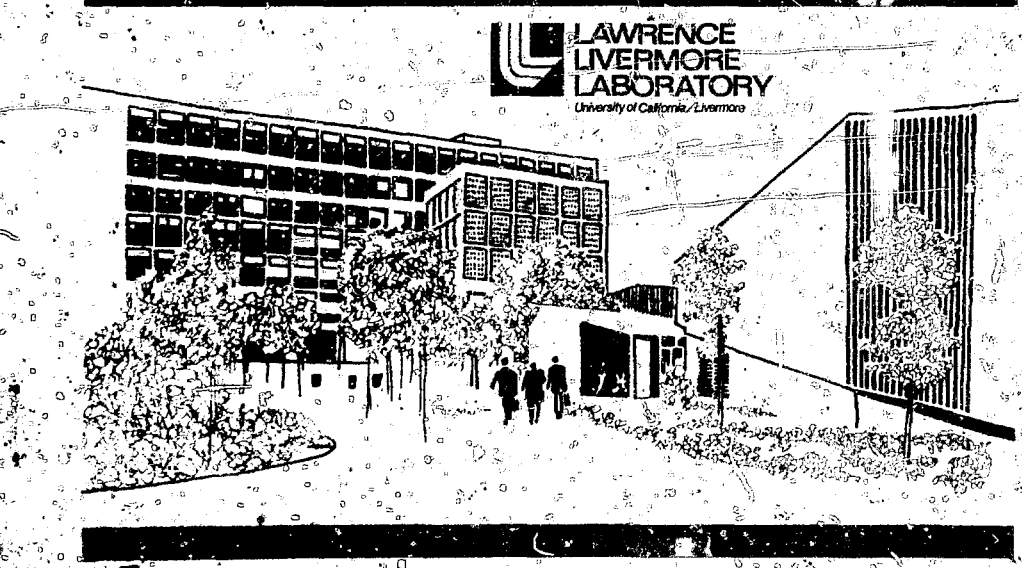

Distribution Category
UC-80

LAWRENCE LIVERMORE LABORATORY
University of California/Livermore, California/94550

UCRL-52265

AN INVESTIGATION OF PRESSURE TRANSIENT PROPAGATION IN PRESSURIZED WATER REACTOR FEEDWATER LINES

S. B. Sutton

MS. date: July 22, 1977

Contents

Contents (continued)

List of Figures

List of Figures (continued)

Nomenclature

A	Pipe cross-sectional area
B	Fluid bulk modulus
C	Fluid sound speed
C_W	Wave velocity
D	Pipe inside diameter
E	Elastic modulus
f	Velocity squared friction factor
$\overline{F}$	Force
g	Gravitational constant
H	Pipe wall thickness
K	Lumped friction factor
$\hat{k}_i$	Elbow direction vectors (Fig. 12)
$\hat{\ell}$	Elbow direction vector (Fig. 12)
L	Slug length
$\hat{m}_1, \hat{m}_2, \hat{m}_3$	Orthoginal coordinate system direction cosines
$\hat{n}_i$	Elbow direction vector (Fig. 12)
P	Pressure
r	Pipe inside radius
R	Elbow radius (Fig. 12)
t	Time
T	Temperature
u	Velocity
v	Volume
$\overline{V}$	Velocity vector
x	Distance
σ	Stress
Δx	Differential distance
Δt	Time increment
ρ	Fluid density
ΔP	Pressure change
ε	Strain
θ	Elbow angle

Nomenclature (continued)

Subscripts

m	Maxium
o	Initial
W	Wave
w	Wall
y	Yield

Superscripts

o	At time zero
n	Time $n(\Delta t)$
n+1/2	Time $(n+1/2)\ \Delta t$
n+1	Time $(n+1)\ \Delta t$

AN INVESTIGATION OF PRESSURE TRANSIENT PROPAGATION IN PRESSURIZED WATER REACTOR FEEDWATER LINES

Abstract

This document reports the results of a study for the Nuclear Regulatory Commission (NRC) to provide a general understanding of pressure transient (water hammer) propagation in pressurized water reactor (PWR) steam generator feedwater piping systems. A typical feedwater network is defined, and pressure transient initiation is discussed, as well as the plausible pulse shapes reported. The analysis is performed by using the computer codes PTA and WHAM. Forces are calculated at elbows and valves by using momentum principles, The effects of pipe yielding, pipe wall friction, and elbow and value losses are included. Pipe yielding and elbow/valve effects are found to be important, and pressure magnitudes and forces are substantially reduced when these effects are included in the analysis. Typical pressure and force time histories are also given.

Section 1
Introduction

This report discusses results of the first phase of a one-year contract* with the Nuclear Regulatory Commission, Division of Operating Reactors (NRC/DOR), for a *generic* investigation of the effect of hydraulic shock or water hammer on the feedwater piping network of pressurized water reactors (PWR).

*Contract No. B&R 20 19 04 02 FIN A0207.

Of the (at least) twenty-four steam generator related water hammer incidences[1] reported to date, the most significant one occurred in 1973 in steam generator No. 22 of the Indian Point No. 2 Nuclear Power Plant.[2] The water hammer caused bulging of the feedwater pipe near the steam generator, and failure of the pipe at the containment wall. Evidence indicated that the water hammer was caused

by the formation and subsequent sudden collapse of a steam bubble in the feedwater line near its inlet to the steam generator. Since then, additional severe water hammers have occured. In particular, a water hammer occured at the Calvert Cliffs Nuclear Power Plant No. 1,[3] which caused failure of two feedwater valves upstream of the steam generator.

It is in response to these incidences that NRC/DOR funded this study to investigate the effects of water hammer on the feedwater network of pressurized water reactors.

Phase I of the contract calls for detailed investigation of the fluid mechanical aspects of pressure pulse propagation. Phase II entails a detailed structural analysis of the feedwater pipe by using results of Phase 1.

By an agreement with NRC,[4] Phase I consisted of three tasks:

1) Select appropriate water hammer pulses, resulting from steam bubble collapse, for use as input to a propagation analysis.
2) Survey and select appropriate propagation schemes for use in the analysis. Include acquired and developed computer software to predict loads that the water hammer places on the system. Also investigate effects that the piping system has on the pressure pulse, i.e., elbow loss, pipe yielding, wall friction.
3) Calculate loads on the piping system due to the pressure transient, and use the results of Items 1 and 2 (above) in this analysis. In conjunction with NRC/DOR personnel, select a representative piping system for use in this generic study.

Section 2
Summary

In Phase I of this contract, we investigated the fluid mechanical aspects of pressure pulse propagation in PWR feedwater systems. To do so, we selected appropriate water hammer pulses for use as input to the propagation analysis.

From the available literature, at least twenty-four PWR steam-generator related water hammer incidences have occurred. At least two of these have caused severe damage to the piping network.

The pressure pulse is believed to be caused by drainage of a horizontal section of pipe at the steam generator inlet. When an upstream valve in the feedwater line is closed, continued boiling in the steam generator causes the water level to drop below the

feedring. Subsequently, "cold" water is injected through the feedwater line to restore the steam generator water level. At some point in time, a steam bubble is trapped in the horizontal section of pipe adjacent to the steam generator. Collapse of this bubble, from condensation, causes an impact of water surfaces and generates the severe pressure pulses experienced.

In conjunction with NRC personnel, we defined a basis feedwater piping network. It consists of approximately 300 ft of 16-in.-o.d. pipe. The pipe is made of SA-106, Class C steel and has a wall thickness of 0.844 in. The pipe section contains fifteen elbows, a flow element, check valve, and plug valve. We obtained properties of the pipe material at elevated temperatures so that its stress-strain curve could be reconstructed.

We found two pressure pulse shapes to be plausible and refer to these as the "Westinghouse" and "Tihange" pulse forms. Both are characterized by a gradual depressurization (approximately 20 ms) and a long dwell period (approximately 40 ms). The depressurization time is associated with steam condensation, creating a comparative vacuum. The dwell period is associated with the time it takes the water surfaces to impact. The elevated pressure portion of the "Westinghouse" form is a single spike of approximately 1.5 ms duration and is used in two forms: square and triangular. The evelvated pressure portion of the "Tihange" form consists of multiple spikes. Each has a duration of approximately 2.5 ms and is triangular in shape.

In addition to variations in pulse shape, we also found justification for variations in pulse magnitude. Both damaging as well as benign water hammers have occurred. In our analysis, we consider peak pressure magnitudes of 3000 and 6000 psi. The lower value is well below the yield point of the pipe while the upper value is well above the yield limit.

The two computer codes used in our analysis — PTA and WHAM — were placed on the LLL computer network. We modified them to extract forces at specified pipe components, account for elbow/valve losses, and produce spacial and time plots of pressure in the piping network. Forces were calculated by using conservation of momentum principles in a pipe component. Elbow/valve losses are accounted for through use of a lumped friction. In our study, we use a lumping factor several orders of magnitude greater than the steady-state value. In addition, during depressurization, the lumped factor is made a function of the pressure gradient. This recognizes that losses are likely to be lower in relatively low-pressure gradient situations. Pipe yielding

is accounted for by reducing the propagation velocity of the pressure wave when the local pressure is greater than the yield pressure.

We performed a series of verification calculations to check the correctness of the computer codes and our loss models. The first series, duplicating a suddenly closing valve, were calculated by using PTA, WHAM and the coupled Eulerian/Lagrangian CHAMP computer code. Calculations were performed for both rigid and elastic walls. The PTA and WHAM calculations compare to within 0.1% of the theoretical answer. The CHAMP calculations, which demonstrated the oscillatory behavior of the pipe wall, compared to within 4% of the theoretical answer.

In addition, we performed test calculations to test the plasticity and elbow models. In both situations, we compared our calculation with experiments. The plasticity calculation demonstrated the reasonableness of the model used in PTA. In the elbow-loss test problem, we found that use of a lumping factor of 1.5×10^4 reproduced the experimental results.

Calculations were performed on our basis feedwater for five cases:

1. "Westinghouse" pulse with a peak pressure of 3000 psi (below yield limit), with no elbow losses included.
2. "Westinghouse" pulse with a peak pressure of 3000 psi (below yield limit), with elbow losses included.
3. "Westinghouse" pulse with a peak pressure of 6000 psi (above yield limit), with elbow losses included.
4. "Tihange" pulse with a peak pressure of 3000 psi (below yield limit), with elbow losses included.
5. "Tihange" pulse with a peak pressure of 6000 psi (above yield limit), with elbow losses included.

For Case 1, which included no losses, the pressure was a constant throughout the piping network. At all 90° elbows, the maximum total force was 6.89×10^5 lb.

For Cases 2 and 4, elbow and valve losses reduced the peak pressure to roughly 45% of its original value. The forces were correspondingly reduced. The depressurization portion of the curve was only slightly affected since the loss factor form was chosen to minimize losses in this region.

For Cases 3 and 5, pipe yielding reduced the peak pressure to the pipe yield pressure (4500 psi) by the time the wave traveled 11 ft, which is well before the first loss elbow. In the case of the Tihange pulse, the plasticity effect also filled in the

valleys between spikes. Before the pulse reached the first elbow, the minimum pressure in the spike portion of the curve was very nearly the operating pressure of the steam generator. This served to reduce the force band in the spike portion. As with Cases 2 and 4, the inclusion of losses at elbows and valves served to substantially reduce the pressure and force magnitudes during the spike portion of the pulse.

Section 3
Water Hammer Phenomenon

To set the scene for pressure transient peneration, a small portion of a typical feedwater system is shown in Fig. 1. A detail of the short horizontal pipe connecting to the feedring is given in Fig. 2.

When a valve upstream in the feedwater system is closed, the flow

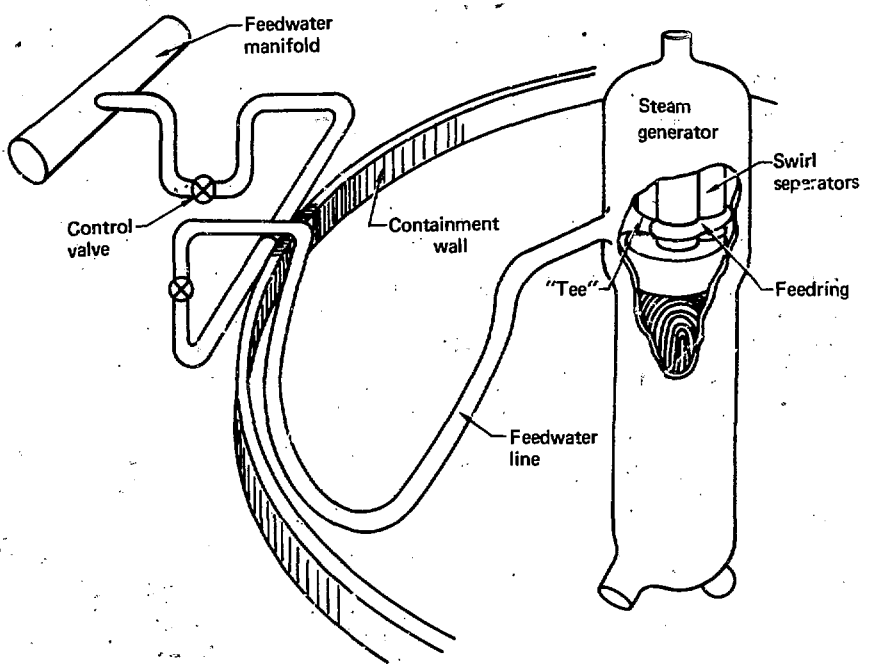

Fig. 1. Layout of PWR feedwater line.

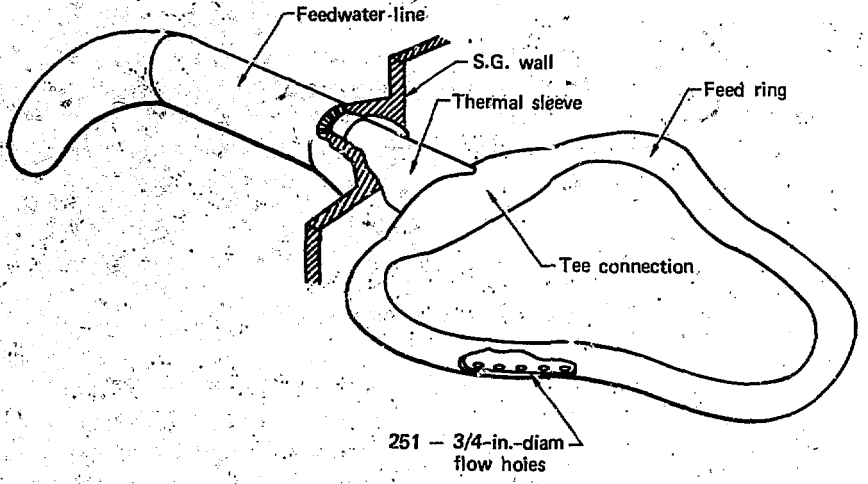

Fig. 2. Steam generator feedring.

in the feedwater line is stopped. Subsequent boiling in the steam generator causes the water level to drop, uncovering the feedring and draining the short horizontal pipe section. At a later time, "cold" auxilary feedwater is injected through the feedwater line to restore the steam generator water level. At this time when the pipe is partially filled, two types of water slugs are possible: "short" or "long".

The short-slug formation is represented in Fig. 3. At some point in time, a surface perturbation at the feedring tee causes formation of a waterslug and isolation of a steam bubble. Subsequent condensation of steam within the bubble, and the resulting pressure differential causes acceleration of the slug down the pipe. Impact of this slug on the downstream water surface and pipe elbow causes the severe pressure waves experienced.

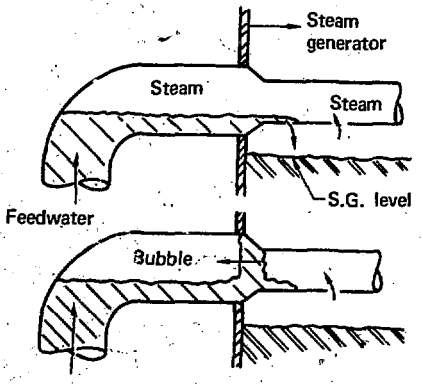

Fig. 3. Representation of "short" slug formation.

The formation of long slugs,[5] as illustrated in Fig. 4, occurs as the water level in the steam generator is restored and the outlet holes in the bottom of the feedring are covered, which traps steam in the feedring and horizontal pipe. Subsequent condensation of this steam "bubble" causes water to be drawn into the feedring and down the horizontal pipe. The impact of this slug against the elbow and water surface causes the severe pressure pulse.

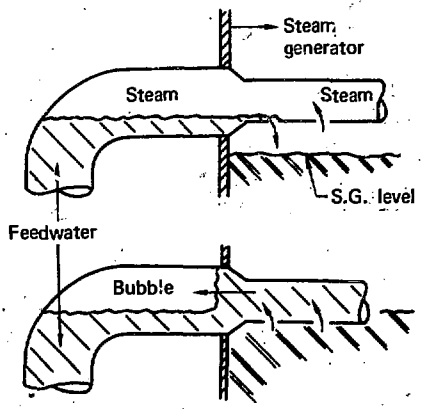

Fig. 4. Representation of "long" slug formation.

Both of these "models" appear to be supported by observed phenomenon. For example, Block et al[1] have generated short slugs in scale model tests. An Indian Point incident report[6] mentions that the water hammer occurred at the time the feedring began to be covered, accompanied by a sudden drop in water level in the steam generator. This would seem to support the long-slug concept where water is drawn back into the feedring from the steam generator.

Section 4
Basis PWR Feedwater Piping Network

FEEDWATER LINE DEFINITION

In consultation with NRC, we have defined a "typical" PWR feedwater system for use in our analysis.[7] A schematic of the piping system is shown in Figs. 5 and 6 and characteristics of the piping network are given in Table 1. Properties of the pipe material and water are discussed in Appendix A. At the time of water hammer, we estimate the fluid and pipe temperature to be 300°F. This is roughly the mean between the plant operating temperature and the cold auxiliary water temperature.

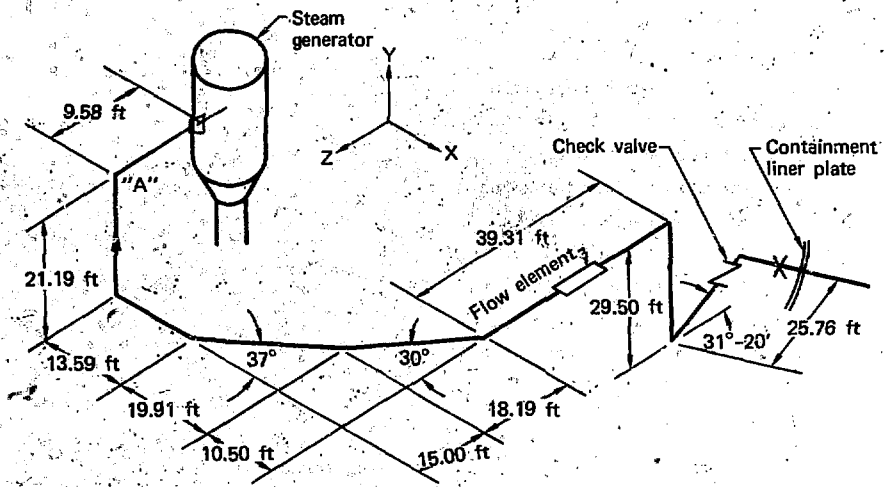

Fig. 5. Schematic of basis feedwater piping network — inside containment.

Table 1. Summary of representative piping system.

Pipe Material Type	SA-106, Type C
Main feedwater pipe diameter	16.0 in. o.d.
Main feedwater pipe wall thickness	0.844 in.
Length of pipe in analysis (from Point A to Point B of Figs. 5 and 6)	~288 ft
Component summary	
Elbows - radius = 2.0 ft	14
Flow element (Venturi type)	1
Check valve	1
Plug valve	1

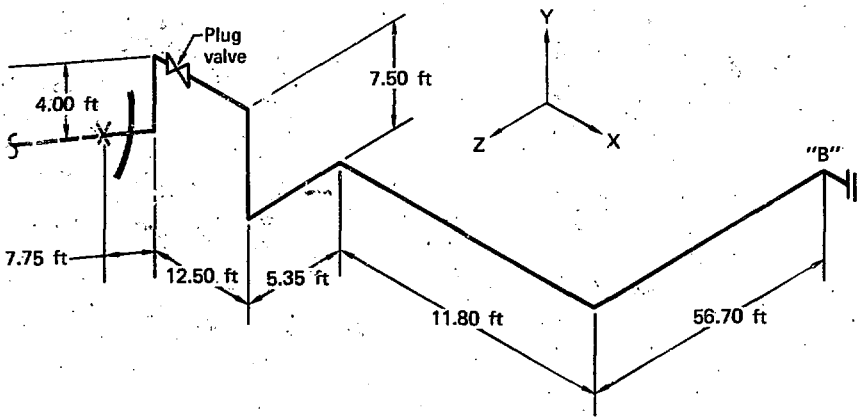

Fig. 6. Schematic of basis feedwater piping network — outside containment.

Section 5
Pulse Selection

BACKGROUND

The first major aspect of this contract was to select water hammer pulses, representing pressure conditions in the immediate vicinity of the steam bubble, for use as boundary conditions in the propagation analysis. As criterian for selecting representative pulses, we conclude that candidate pulses should:

- Be consistent with observed phenomenon. Pressure measurements have been made on the full size Tihange Feedwater System[8] as well as scale model experiments.[1]
- If possible, be consistent with present theories. Simple models have been proposed to provide magnitude estimates of this phenomenon.[1,5]
- Cover the broadest possible range of shape and magnitude. Observations in operational steam generator systems indicate that very benign water hammers may occur, in addition to the more violent type that concerns us in this study.[2]

CANDIDATE PULSE SHAPES

Our study revealed that there are basically two acceptable pulse shapes: "single" and "multiple" spikes

(Fig. 7). The "single spike" pulse is used in two basic shapes: the solid-line or square pulse, typically used in "vendor" analysis of water hammer phenomenon[8]; the dashed-line or triangular pulse, observed in the Block et al. experiments.[1]

The "multiple spike" has most recently been discussed by Vreeland,[5] and has some experimental basis in the experiments conducted at the Tihange Nuclear Facility in Belgium.[8] The experimental traces recorded at Tihange are given in Fig. 8.

Both pulses are characterized by the gradual depressurization (t_1) and a rather long dwell period (t_2). These aspects are associated with the very rapid condensation of steam in the bubble which creates a comparative vacuum. The total depressurization time ($t_1 + t_2$) is the time the slug (whether finite or long) takes to traverse the original bubble length.[1,5] Beyond this point, the two pulses are markedly different. In both instances the pressure increases suddenly (as compared to the depressurization rate) to a magnitude P_m as the water slug impacts the "stationary" surface. In the available literature, the single spike pulse is associated with the short-slug situation. The pulse duration is the time it takes the impact pressure to transit the slug, reflect at the back end, and for the resulting rarefaction to return to the impact surface. Thus, this time may be described as

$$\Delta t = \frac{2L}{C_w} . \qquad (1)$$

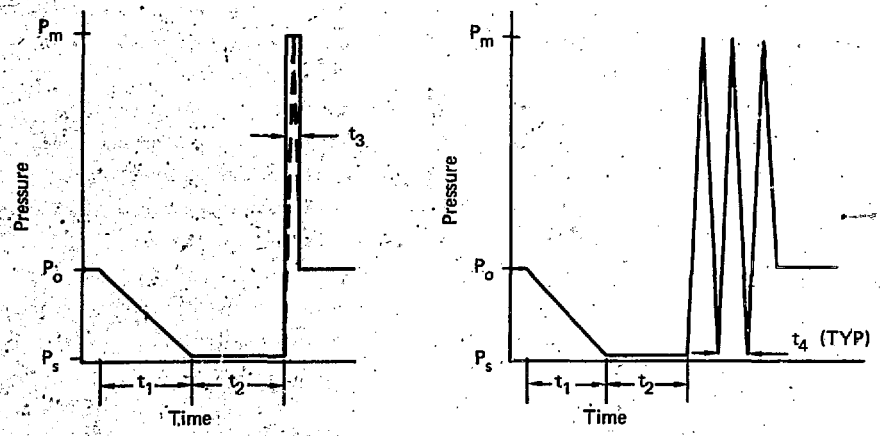

Fig. 7. Candidate pulse shapes.

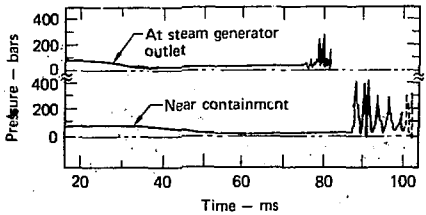

Fig. 6. Pressure histories from Tihange tests.[8]

In addition, Weeland recently associated the multiple spike pulse with the long slug situation.

The time parameters (t_1 and t_2) are difficult to accurately predict. The depressurization rate depends on the bubble condensation rate. This is highly influenced by steam/water interface conditions, water temperature, and water flow rate. In turn, the "dwell" time (t_2) and pressure magnitude (F_m) are dependent upon the pressure difference between the bubble and steam generator (P_o), and the slug length and slug growth rate. For this reason, a simple theory has yet to evolve that will provide complete definition of the water hammer pressure pulse.

We also conclude that in addition to variations in pulse shape, pulse magnitude must also be considered a variable. In several instances at Indian Point[2], the pulse magnitude was small enough that no discernable pipe damage was evidenced. However, in another instance,[2] the water hammer pulse was of a magnitude sufficient to cause pipe yielding near the steam generator. To the first order, the yield pressure of the pipe is given by thin-wall pipe theory:

$$P_y = \frac{\sigma_y H}{r} \quad . \qquad (2)$$

The parameters used in our analysis are described in Table 2. Because available theories fail to completely predict a reasonable pulse, our selections are combinations of theory, experiment, and recommendations found in the literature. The depressurization times (t_1 and t_2) are based on the Tihange trace characteristics and are appropriate for this analysis since the length of the horizontal pipe entering the steam generator at Tihange is comparable to that in our

Table 2. Pressure pulse parameters.

Depressurization time (t_1)	20 ms
Dwell time (t_2)	40 ms
"Westinghouse" pulse duration (t_3)	1.5 ms
"Tihange" pulse duration (t_4)	2.5 ms
Steam generator base pressure (P_o)	900 psi
Minimum pressure (Ps)	67 psi
Maximum pressure (Pm) - elastic case	3000 psi
yield case	6000 psi

typical piping system. Time t_3 of the Westinghouse trace is representative of the pulse length used by vendor analysis.[8] Time t_4 of the Tihange pulse is representative of the pulse length observed in the Tihange Tests.[8] The peak-pressure range was selected to include pressures well below the pipe yield limit as well as above the pipe yield limit.

Finally, it should be noted that the pulse shapes, as shown in Figure 7, are approximate and highly speculative. The definative study investigating the initiation phenomenon has yet to be performed.

Section 6
Computation Schemes for Pressure Propagation

BACKGROUND

The purpose of this task was to determine the most appropriate method for propagating the pressure transient through the piping system. A typical approach applied to propagating a pressure pulse through a PWR feedwater piping system has been merely to apply the specified pressure pulse at the elbows where forces are desired.[8] Forces are obtained by integrating the pressure over the elbow surface area. A basic assumption in this type of analysis is that the pressure pulse maintains the same shape and magnitude throughout the piping network. In addition, the structure is regarded as perfectly rigid. Thus, pressure changes associated with global pipe motion are neglected.

In performing a best-estimate generic analysis, we felt that it is important to predict realistic pulse behavior as it transits the pipe network. This requires modeling the various mechanisms that alter pulse shape and magnitude which necessitated using a fluid-mechanics calculation in our analysis. Among the loss mechanisms deemed important are plasticity effects (pipe yielding), elbow/valve loss, and pipe friction. By considering loss mechanisms, we are in effect investigating the conservatism in the analytical approaches where no losses are considered.

Appreciable work has been performed in analyzing the pressure surge caused by sudden closure of a valve in pipelines.[9-11] However, few of the techniques discussed consider loss mechanisms. In particular, elbow losses are generally ignored since either the systems under consideration involve long straight sections of pipe with few elbows and valves, or the presence of liners or

orifices completely overpower the effect of elbows and valves.

Virtually all of these studies use some form of the method of wave superposition, as discussed by Parmakian,[10] to solve the transient water hammer equations:

$$\frac{\partial P}{\partial x} = -\rho \frac{\partial u}{\partial t} \text{ (momentum)}, \quad (3)$$

$$\frac{\partial P}{\partial t} = -\rho C^2 \frac{\partial u}{\partial x} \text{ (continuity)}. \quad (4)$$

Equation 3 is a form of the Navier-Stokes equation for one-dimensional flow where the advection and friction terms are neglected. When considering friction in the flow, it is common practice to include the advection terms so that the one-dimensional equations take the form,[12,13]

$$\rho\left(\frac{\partial u}{\partial t} + u \frac{\partial u}{\partial x}\right) + \frac{\partial P}{\partial x} + \frac{f\rho u|u|}{2D} = 0 \text{ (momentum)}, \quad (5)$$

$$\rho C^2 \frac{\partial u}{\partial x} + \frac{\partial P}{\partial t} + u \frac{\partial P}{\partial x} \approx 0 \text{ (continuity)}. \quad (6)$$

These equations are typically solved by using the method of characteristics. More will be said on these solution techniques later.

SOLUTION SCHEMES

To perform this analysis, we obtained two computer codes; PTA[14] and WHAM.[15] Both codes are operating on the Lawrence Livermore Laboratory CDC 7600 computer system. Both computer codes assume that the piping network is rigidly fixed in space. Thus, the pressure changes associated with motion of the pipe caused by hanger deflection cannot be considered. The details of each of these computer codes are discussed below.

PTA Computer Code

Below is a brief summary of the features of the PTA computer code as used in our analysis. Included are the original features as well as features we have added. The version of the PTA we obtained:

- Is applicable to complex three-dimensional networks of one-dimensional pipes, and accounts for junctions, elbows, pumps, deadend pipe sections, and rupture discs,
- Uses method of characteristics to solve Eqs. 5 and 6,
- Treats continuous pipe friction by using steady flow friction factors,
- Calculates velocity and pressure at all nodal points.

- Accounts for inelastic behavior of pipe material.

In addition, we added the capability to:

- Account for high loss components such as elbows.
- Calculate time-dependent forces at specified components.
- Produce spacial plots of pressure and time-history plots of pressure.

The implementation of PTA on the LLL computer network and the addition of new capabilities were performed completely under this contract. A summary of the PTA solution scheme is given in Appendix B.

WHAM Computer Code

Below is a brief summary of the features of the WHAM code as used in our study. Included are the original features as well as features we have added. The version of WHAM we obtained:

- Is applicable to complex three-dimensional networks of one-dimensional pipes, and accounts for junctions, elbows, pumps, and deadend pipe sections.
- Uses the method of wave superposition to solve Eqs. 3 and 4.
- Accounts for pipe friction by using discrete orifices.
- Calculates velocity and pressure at all nodal points.
- Accounts for elastic behavior of pipe material.

In addition, we added the capability to:

- Account for high loss components such as elbows.
- Calculate time dependent forces at specified components.
- Produce special plots of pressure and time history plots of pressure.

The impementation of WHAM on the LLL computer network and the addition of new capabilities were performed completely under this contract. A summary of the WHAM solution method is given in Appendix B.

FORCE CALCULATIONS

The goal of the fluid analysis work done in this contract was to provide force input for Phase II of the contract (structural analysis). We elected to calculate forces within the pipe network using the standard application of Newtons second law.[16] In considering flow within an arbitrary control volume (Fig. 9), the force which acts on the fluid is given

* This feature is highly computer-system dependent. The graphics capability added is a feature of the Lawrence Livermore Laboratory computer system and is not transferable to other computer systems.

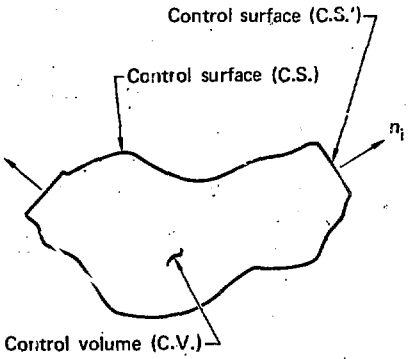

Fig. 9. Pipe component control volume.

$$\overline{F} = \iint_{C.S.} \overline{V}\,(\rho\overline{V} \cdot d\overline{A}) + \frac{\partial}{\partial t}\iiint_{C.V.} \rho\overline{V}dv \quad . \quad (7)$$

We may consider the total force $\overline{F}$ to be composed of forces which act on the solid boundaries of the control volume (friction forces, pressure) and forces which act over the inlet and outlet planes to the control volume. Now, if we define C.S. to be that portion of the control surface represented by the inlet and outlet planes, we may write the forces acting on the control volume walls as

$$\overline{F}_w = -\iint_{C.S.} P d\overline{A} + \iint_{C.S.} \overline{V}\,(\rho\overline{V} \cdot d\overline{A}) + \frac{\partial}{\partial t}\iiint_{C.V.} \rho\overline{V}dv \quad (8)$$

Equation 8 is the basic force equation used in both PTA and WHAM.

We should note that $\overline{F}_w$ is a vector with magnitude and direction. The best method to resolve the direction of this vector in an orthogonal coordinate system is to determine the three vector components of $\overline{F}_w$. Let us consider $\hat{m}_1$, $\hat{m}_2$, and $\hat{m}_3$ to be the three unit vectors for the orthogonal 1, 2, 3, coordinate system. Thus, we may say:

$$\overline{F}_i = \overline{F}_w \cdot \hat{m}_i = -\iint_{C.S.} P(d\overline{A} \cdot \hat{m}_i) + \iint_{C.S.} (\overline{V} \cdot \hat{m}_i)\,(\rho\overline{V} \cdot d\overline{A}) + \frac{\partial}{\partial t}\iiint_{C.V.} \rho(\overline{V} \cdot \hat{m}_i)dv \quad i = 1,2,3 \quad . \quad (9)$$

Equation 9 is applied at all elements where the fluid imposes a force on the pipe network (elbows, valves, etc.) For example, let us consider an elbow, as shown in Figs. 10a and 10b having an elbow angle θ, radius of curvature R, and pipe radius r in an X,Y,Z coordinate system. In Fig. 10b each of the large "dots" represents a nodal point in the calculation, and the [illegible]ted lines denote boundaries of th[illegible]ol volumes that surround the nodes. The surface integrals are applied at the elbow entrance and exit planes. The volume integration and time

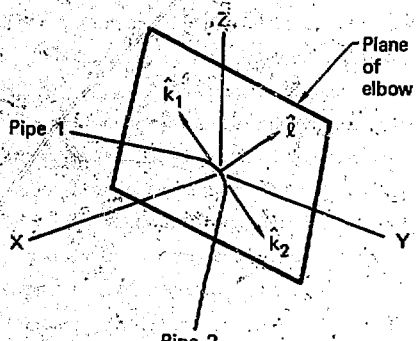

10a. Elbow orientation

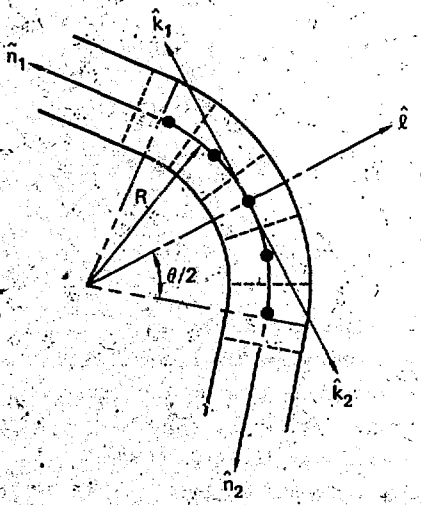

10b. Elbow detail

Fig. 10. Elbow geometry used in force calculation.

differencing are performed for each of the nodal point control volumes and are summed. Further details are given in Appendix C.

LOSS MECHANISMS

As mentioned earlier, we consider pipe friction, pipe yielding, and elbow/valve losses as candidate loss-mechanisms which are discussed in detail below.

Pipe Friction

It is generally regared that wall friction effects are small in systems involving relatively inviscid fluids like water. Several numerical studies, using steady-state friction factors to model transient effects, have demonstrated the small effect that this friction model has on pressure transients in water-filled pipes.[17,18] More advanced work has been performed which calculates transient friction factors by relating the wall shear stress in transient pipe flow to the instantaneous mean velocity and past velocity changes.[19] However, this type of analysis is impractical in most numerical applications because of large storage requirements necessary to capture the past velocity history. Thus, investigators still rely on the simple steady-state friction factor to model this effect.[14,15]

We continue with this approach in our study. In PTA, which solves Eqs. 5 and 6, we account for pipe friction through use of the steady-state friction factor that is

proportional to the square of the fluid velocity. WHAM, however, accounts for frictional effects through use of Bernoulli's equation where we can say that the pressure loss is given by

$$\Delta P = \frac{f\Delta x}{2Dg} u^2 \quad . \qquad (10)$$

As with PTA, f is the steady-state velocity-squared friction factor. Typically, the factor f is determined from a correlation equation such as the Darcy-Weisbach friction factor relation.

Pipe Yielding

In systems where pressure magnitudes may cause the pipe wall stresses to exceed the material yield point, plastic behavior causes substantial energy loss. In essence, pipe wall yielding causes the pressure transients magnitude to decrease to the yield pressure. We define yield pressure to be the pressure required to cause yield stresses in the pipe. This effect has been demonstrated in several experiments.[20-22] These effects have been modeled by several researchers including two-dimensional modeling by Chang[23] and one-dimensional modeling by Fox.[24]

The method discussed by Fox[24] is used by Youngdahl in PTA.[12,14] Basically, the approach in one-dimensional flow is to modify the wave velocity. In a deformable pipe, we can write the wave velocity C_W as[12,14,24]

$$C_W = \left[\frac{1}{C^2} + \frac{\rho D}{H\left(\frac{d\sigma}{d\varepsilon} - 2\sigma\right)}\right]^{-1/2} \quad . \qquad (11)$$

For an elastic state in the pipe material, the elastic modulus is typically very much larger than the circumferential stress. Thus, Eq. 11 reduces to

$$C_W = \left[\frac{1}{C^2} + \frac{\rho D}{HE}\right]^{-1/2} \quad , \qquad (12)$$

or

$$C_W = \left[\frac{B/\rho}{1 + (BD/HE)}\right]^{-1/2} \quad . \qquad (13)$$

This is the classical elastic propagation velocity discussed by Streeter.[9]

Inherent in this type of model are the following assumptions:

- Pipe yielding is small, i.e., there is negligible change in the pipe diameter.
- Equilibrium exists between the fluid and the pipe wall.
- The pipe is treated as having a thin wall, e.g., there is negligible variation in circumferential stress across the thickness of the pipe.

In most practical applications where pipe failure is not expected the first assumption poses no restriction. The second assumption probably results in an overprediction in the attenuation since the wall stress state will typically lag the fluid pressure state. In PWR feedwater pipe networks, the pipe thickness is generally about 5% of the pipe diameter. Thus, the assumption of thin wall-pipe behavior is reasonable.

Elbow and Valve Losses

In steady-state flow situations, elbows and valves produce significantly larger pressure losses than a straight section of pipe of the same length. The effects are primarily viscous, and result from boundary layer separation initiating recirculation regions. Lacking is a complete understanding of the mechanisms producing elbow and valve losses in transient applications such as water hammers. These losses, however, are most probably a combination of viscous effects and shock reflection.[25]

In most previous applications, it has been assumed that elbow and valve losses are small. This statement has its basis in applications to systems where the effects of orifices and sudden area changes, etc., overpower the effect of elbows. As a result, elbow losses are ignored in virtually all transient applications. It has been demonstrated that in situations where the only substantial loss mechanism present is elbow losses, the effect can be substantial.[22,25] Of particular interest is the recent work of Romander et al.[22] They demonstrate that in a 90° elbow with a pipe radius of 1.5 in. and a radius of curvature of 4.5 in. that the pressure loss may be as great as 15%. For application to feedwater systems, where we deal with long sections of constant area pipe, this is clearly not insignifcant. These results are confirmed by the work of Swaffield.[25] Neither of these papers can be considered a definitive treatise on the subject of elbow losses. Lacking is work to determine if the loss is strongly dependent upon pulse shape. Of particular interest to us would be information on loss as a function of the ratio of pulse length to elbow length as well as pulse-pressure rise rate.

Few people will deny that the flow associated with propagation of a pressure transient through an elbow or a valve is highly three-dimensional. Since the two computer codes used in this analysis are one-dimensional, we are faced with the task of modeling a three-dimensional phenomenon one-dimensionally. Several investigators have suggested that in transient situations, the loss effect should be modeled as it is in steady-state

situations.[26,27] In essence, the approach is to replace the factor f in Eqs. 8 and 15 by f(1+K) where K is the lumped effect. In steady state, it is thought of as the equivalent length of straight pipe required to cause the same pressure loss. They suggest using the steady-state value for K in transient applications which leads one again to the conclusion that elbow and valve losses are small.

Although we have followed the same modeling approach, we depart from past approaches in several ways:

- Since for our force calculations we recognized the existence of several nodes within the elbow or valve (Fig. 10b), we distributed the lumped factor over several nodes on the basis of volume fraction.
- We used a lumping several orders of magnitude larger than steady-state flow to reproduce the effects of Romander et al.[22] Specific details are given in Appendix D and Section 6.

For the portion of the pulse above the steam generator base pressure, the full lumped factor is used. For that portion below the base pressure, the loss factor is a function of the pressure gradient. This recognizes that the losses are likely to be larger in the presence of very rapid pressure changes than in more gradual transients.*

CODE VERIFICATION CALCULATIONS

To verify the calculational correctness of the LLL versions of PTA and WHAM, we performed a series of benchmark calculations. Included were problems to test the basic computational scheme, elbow loss modeling, and the plasticity modeling in PTA. Details of this analysis are given in Appendix D.

*This subject is briefly discussed in comments at the end of the Swaffield paper.[25]

Section 7
Pressurized Water Reactor (PWR) Feedwater Line Analysis

DEFINITION OF PWR CALCUATIONS

In line with the pulse variations discussed in Section 5, five basic PWR problems were considered. All employ the basis feedwater piping network illustrated in Figs. 5 and 6. However, variations in pulse shape

and pulse magnitude are included. The five problems are:

- "Westinghouse" pulse (Fig. 7a) with a peak pressure of 3000 psi (below yield limit) and with elbow losses excluded.
- "Westinghouse" pulse (Fig. 7a) with a peak pressure of 3000 psi (below yield limit) and with elbow losses included.
- "Westinghouse" pulse (Fig. 7a) with a peak pressure of 6000 psi (above yield limit) and with elbow losses included.
- "Tihange" pulse (Fig. 7b) with a peak pressure of 3000 psi (below yield limit) and with losses included.
- "Tihange" pulse (Fig. 7b) with a peak pressure of 6000 psi (above yield limit) and with elbow losses included.

In our analysis, we included lumped losses and calculated forces at 16 locations in the basis piping network. These locations are shown in Figs. 11 and 12. A summary of these loss and force components are given in Table 3.

CALCULATION OF LOSS FACTORS

Having verified that the increased lumped friction factor is a reasonable approach to modeling dynamic losses of a shock wave in an elbow (Section 6 and Appendix D), we were left with the task of selecting appropriate factors for the elbows and valves.

We use the elbow loss calculation of Appendix D as code calibration.

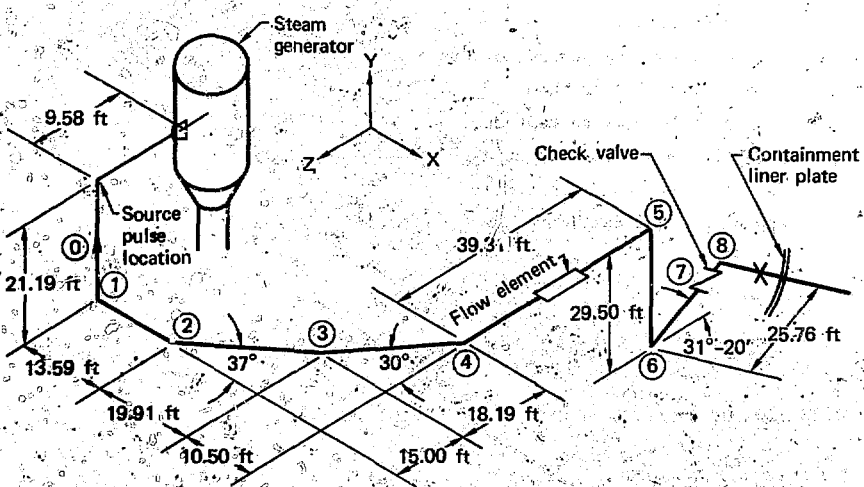

Fig. 11. Piping network loss and force locations — inside containment.

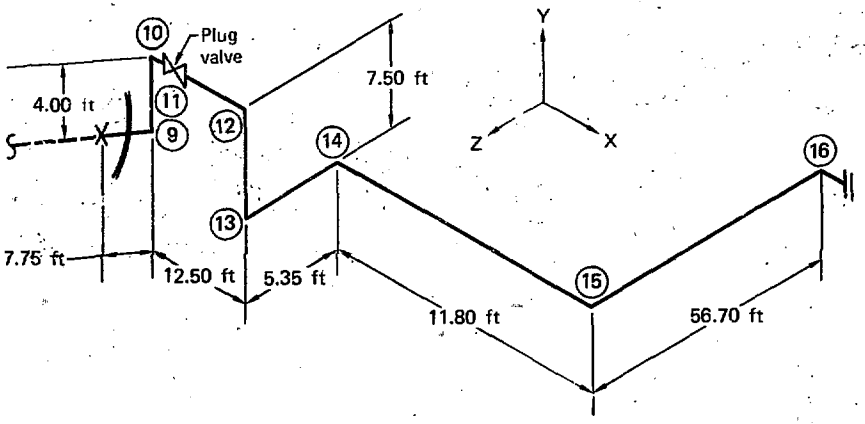

Fig. 12. Piping network loss and force locations — outside containment.

Table 3. Force and loss component summary.

Component	Description
1	90° elbow, R/r = 3.35
2	37° elbow, R/r = 3.35
3	23° elbow, R/r = 3.35
4	30° elbow, R/r = 3.35
5	90° elbow, R/r = 3.35
6	90° elbow, R/r = 3.35
7	Check valve, tilting disc type
8	73° elbow, R/r = 3.35
9	90° elbow, R/r = 3.35
10	90° elbow, R/r = 3.35
11	Valve, plug type
12	90° elbow, R/r = 3.35
13	90° elbow, R/r = 3.35
14	90° elbow, R/r = 3.35
15	90° elbow, R/r = 3.35
16	90° elbow, R/r = 3.35

From the Crane Data Book,[28] the overall steady-state loss factor for a bend is given by

$$K_B = (n - 1)(0.25\pi \frac{r}{D} + 0.5 K_{90}) + K_{90} , \quad (14)$$

where

$$n = \frac{\text{bend angle}}{90°} .$$

For a bend of 90° with R/r = 3.16 (Romander Elbow);

$$K_{90} = 15.37 \quad (15)$$

Thus, compared to the value of 1.5×10^{-4} used in the elbow loss calculation of Appendix D the dynamic lumping is 976 times the steady-state

lumping factor. This magnification factor of 976 was used to generate dynamic lumping factors from steady-state factors for the other components.

The elbows in our basis piping network have R/r = 3.35. From the Crane Data Book,[28] a 90° elbow of this type has

$$K_{90} = 14.58 \ .$$

Steady-state loss factors for the other elbows are calculated by using Eq. 14. The modeling of the check valve is much more difficult. In the presence of a pressure transient, the disk position may vary from fully closed to fully open. The exact behavior of the ckeck valve during a pressure transient is not well understood. In particular, the dynamic loss characteristics have not been characterized. It is anticipated that the more restrictive the valve is, the more important reflections are as an attenuation mechanism. To be consistent with the loss modeling developed for this study, which is based on vicous loss theory, we have elected to treat the check valve as fully open. In this configuration, reflection effects are negligible. This steady-state loss factor of 135 for the fully open check valve was obtained from NRC personnel.[29] It should be noted that this configuration will result in greater forces on the downstream components because attenuation will be lowest in the fully open configuration. The other possible extreme would be to consider the check valve as fully closed. This would maximize loads on the upstream section of plane. However, this would eliminate loading on the downstream portion. This is not consistent with observed phenomenon. In at least one instance[3] severe damage occurred beyond the check valve. We conclude that the fully open configuration is the more correct approximation. The steady-state loss factor for the plug valve was obtained from the Crane Data Book.[28] The steady-state factor for this valve is given by

$$K_v' = \frac{K_s' + [0.8(1-\beta^2) + 2.6(1-\beta^2)^2] \sin\frac{\gamma}{2}}{\beta^4}, \qquad (16)$$

where

$$K_s' = 8f \ , \qquad (17)$$

$$\beta = d_1/d_2 \ .$$

For our particular valve, as specified by NRC/DOR, d_1 = 11.75 in., d_2 = 14.31 in., and γ = 9.27 degrees. Since f is approximately 0.013 for a 14.31-in.-i.d. pipe, the stead-state factor is

$$K_v' = 25 f \ .$$

Thus, K = 25.

A summary of the steady-state loss factors and their dynamic counterparts used in our analysis are given in Table 4.

Table 4. Loss factors.

Component	Steady state loss factor (K)	Dynamic loss factor
90° elbow	14.58	1.42×10^4
73° elbow	12.95	1.26×10^4
37° elbow	9.51	9.28×10^3
30° elbow	8.84	8.63×10^3
Gate valve	24.96	2.44×10^4
Check valve	135.	1.318×10^5

DISCUSSION OF CALCULATION RESULTS

To discuss the five cases, we will present pressure and force traces at key locations. The key pressure locations are the source junction, and downstream* of Junction 16. We will also discuss the forces at Junctions 1 and 16.

Results for Problem 1 are given in Figs. 13 and 14. In Fig. 13, the pulse applied at the source is given. Since Case 1 is a no loss case, the pressure trace remains unaltered as it transits the piping network. The forces applied to the piping network at Location 1 are given in Fig. 14.

*The downstream side of a junction is the side farthest from the steam generator.

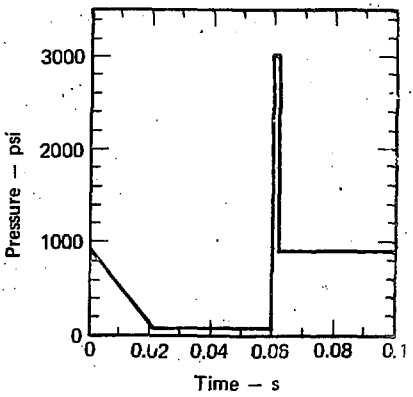

Fig. 13. Case 1 — Pressure pulse applied at source junction.

The peak total force is 6.9×10^5 lb, being equally distributed between the X- and Y-directions. Because of the elbow orientation, the Z-direction force is zero. This same total force will be seen at all other 90° elbows in the system.

Results for Case 2 are given in Figs. 15 through 17 and Table 5. In Fig. 15, we see the effect that our elbow and valve loss model has on the pressure pulse. After transiting the piping system, the peak pressure is reduced to 46% of its original magnitude. This represents an average pressure loss of 5% at each loss component. A detailed look at pressure values at several of the system components (Table 5) shows that the loss is highest at the first elbow, and tapers off as the pulse changes magnitude and shape (top becomes rounded).

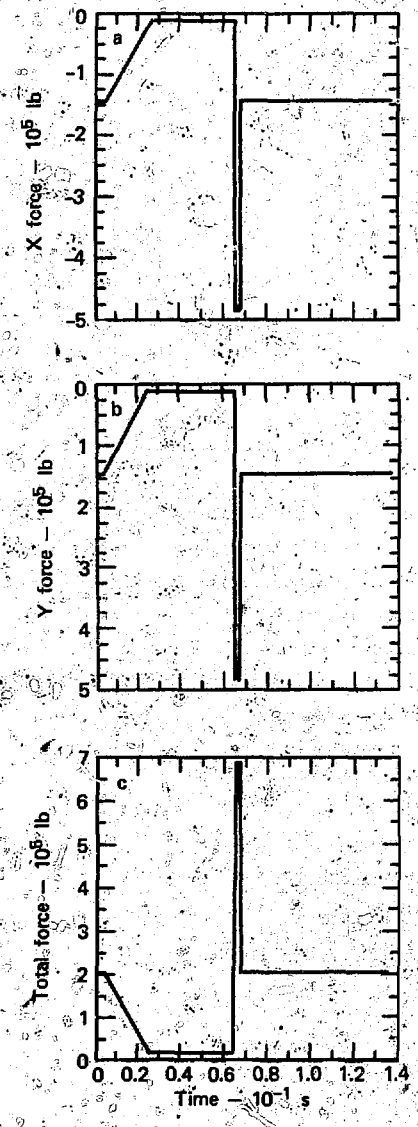

Fig. 14. Case 1 — forces at Junction 1 (note: Z force equals zero).

In addition, it is important to note that the individual losses experienced in this calculation are not as large as in the calculation of the Romander experiment. Possible explanations for this are

- In our elbow/valve loss model, the losses are basically viscous. Since the basis network temperature is 230°F greater than the temperature of the Romander experiments, the friction factor will be lower in the basic network calculations.
- In commercial pipe, the surface roughness is relatively insensitive to pipe diameter. Thus, the surface roughness to pipe diameter is greater for the Romander pipe than our basis pipe, and the friction factor will therefore be greater in the Romander pipe.

In addition, based on Swaffield's work,[25] the losses can be expected to be lower for an elbow with a greater radius ratio (R/r). It should also be noted that the pressure during the depressurization and dwell periods was only slightly affected by the lumped friction since in these regions the loss factor was taken as a function of the pressure gradient. Another important consideration is the reflection phenomenon produced by our lumped friction model. As the pulse

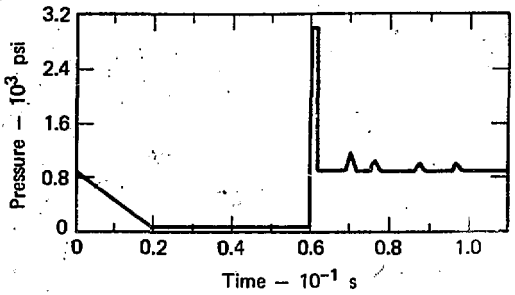

Pressure at source junction

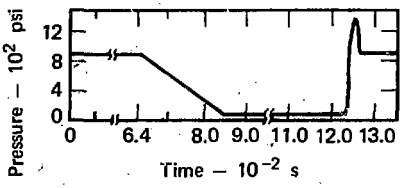

Pressure downstream of location 16

Fig. 15. Case 2 — representative pressure traces.

transits an elbow, a reflected wave is sent back through the piping network (traveling in a direction opposite the main wave). These reflected waves appear quite vividly on the pressure traces of Fig. 15. This behavior seems quite plausible to us since some sort of reflection might be expected when a wave moves through a component that represents either an area change or a direction change. The forces at Locations 1 and 16 are given in Fig. 16 and 17, respectively. As with the pressure, the peak total force is significantly reduced through the inclusion of elbow/valve losses. In Fig. 16, the peak magnitude of the Y force (parallel to entrance leg) is notably greater than the magnitude of the X force (parallel to exit leg). This force change is caused by the pressure loss through the elbow. The same behavior is observed in the forces at Location 16.

Results for Case 3 are given in Figs. 18 through 20 and Table 5. In Fig. 18, we have additionally given the pressure trace midway between the source junction and Location 1. By this point, the peak pressure has been reduced to the yield pressure. The remainder of the results are qualitatively the same as for Case 2.

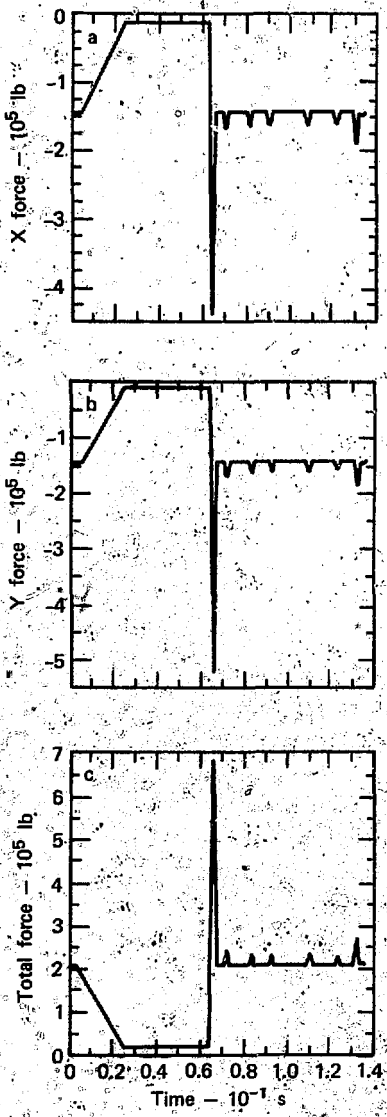

Fig. 16. Case 2 — forces at Junction 1 (note: Z force equals zero).

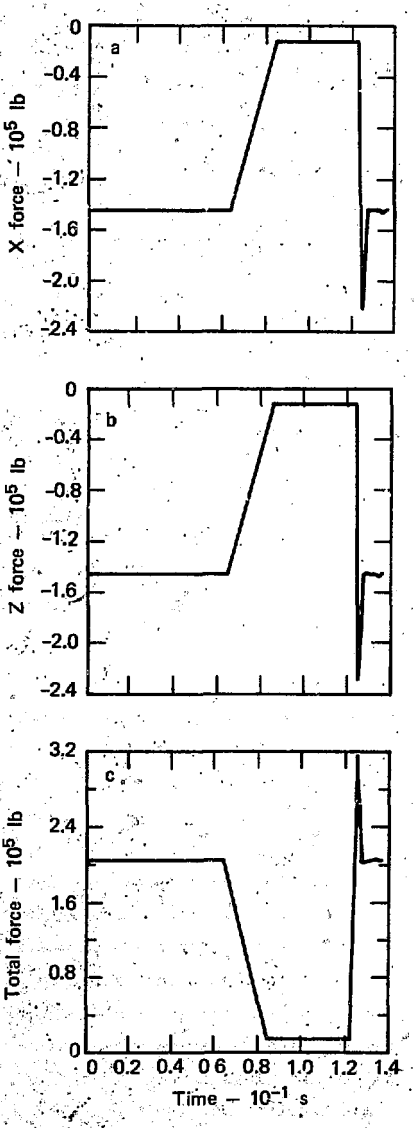

Fig. 17. Case 2 — forces at Junction 16 (note: Y force equals zero).

Table 5. Peak pressure summary.

Junction	Peak pressure downstream[a] of junction				
	Case 2	Case 3	Case 4 (PTA)	Case 4 (WHAM)	Case 5
1	2735	3694	2657	2755	3997
2	2601	3400	2455	2518	3396
3	2456	3108	2309	2358	3102
4	2362	2926	2207	2253	2921
5	2206	2643	2050	2088	2632
6	2082	2437	1938	1958	2418
8	1639	1799	1564	1460	1839
9	1602	1762	1523	1429	1802
10	1561	1677	1517	1412	1766
12	1481	1578	1455	1346	1647
13	1450	1544	1413	1320	1576
14	1431	1512	1398	1308	1548
15	1409	1484	1369	1283	1498
16	1385	1456	1347	1268	1467

[a]The downstream side of a junction is the side farthest from the steam generator

However, at the same locations, the pressures and forces in Case 3 are greater because the pressure pulse going into the elbow at Location 1 is significantly greater in Case 3.

Results for Case 4 are given in Figs. 21 through 26 and Table 5. It is here that we present comparative results for PTA (Figs. 21 through 23) and WHAM (Figs. 24 through 26). In both instances, the results for this triple spike case are qualitatively very similar to the single spike Case 2. Again, we see the presence of reflected waves. However, in this case they come in triples since there are three spikes in the main wave. The PTA and WHAM calculations compare very favorably. The WHAM calculation shows slightly more loss than the PTA calculation (3% more), but this difference overall is quite minor.

Results for Case 5 are given in Figs. 27 through 29 and Table 5. The results for this case are qualitatively very similar to Case 3. However, from the pressure trace at the location midway between the source and Location 1, the third spike of the pressure pulse has not yet dropped below the yield pressure. Thus, one would expect minor bulging of the pipe up to this location. As with Cases 2 and 3, the pressure and force

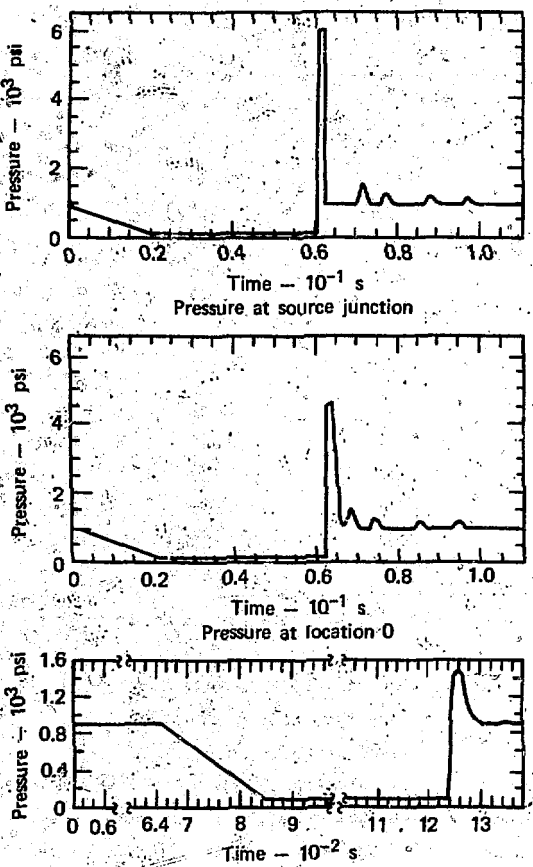

Fig. 18. Case 3 — representative pressure traces.

magnitudes throughout the pipe in Case 5 are greater than in Case 4 since the pressure going into the elbow at Location 1 is greater in Case 5. You will also note that pipe yielding fills in the "valleys" of the multiple spike pulse. Thus, the range of the pressure/force oscillation in the spike portion of the curve is reduced.

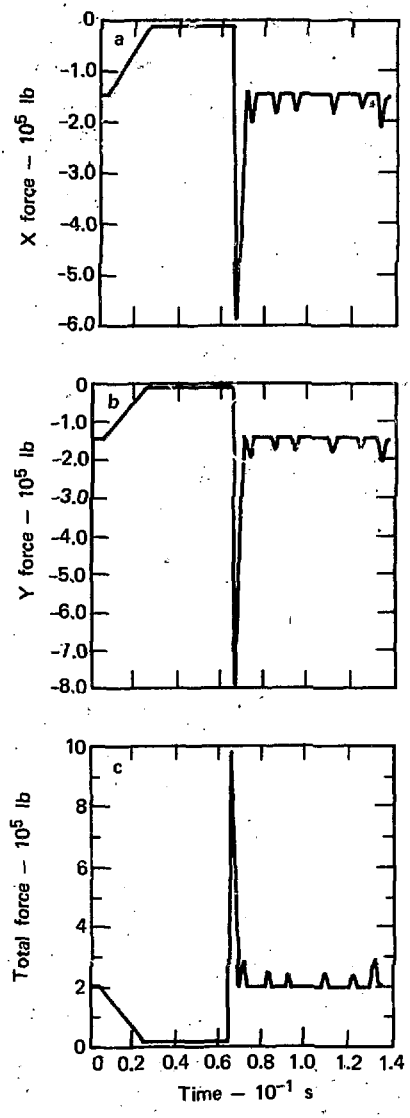

Fig. 19. Case 3 — forces at Junction 1 (note: Z force equals zero).

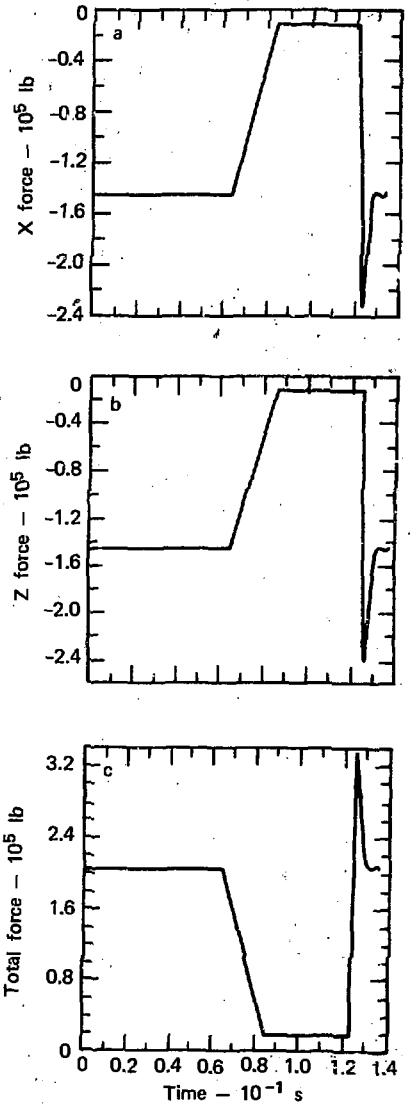

Fig. 20. Case 3 — forces at Junction 16 (note: Y force equals zero).

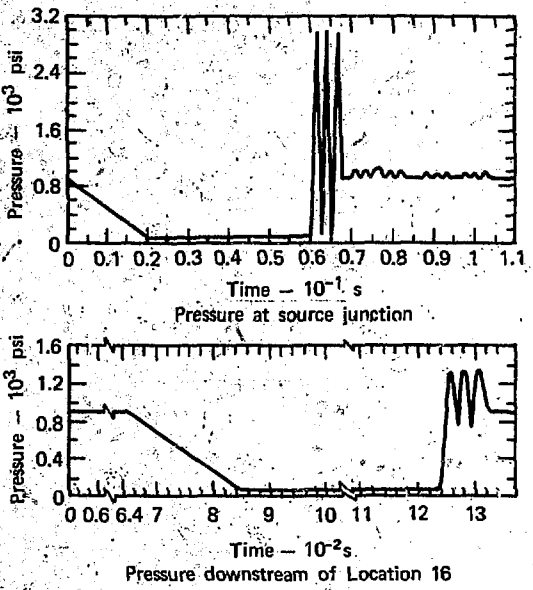

Fig. 21. Case 4 -- representative pressure traces, PTA calculation.

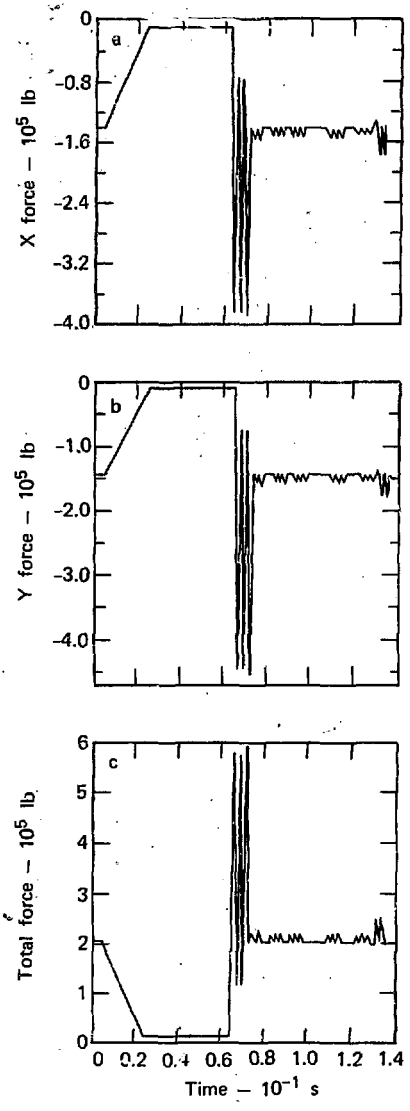

Fig. 22. Case 4 — forces at Junction 1, PTA calculation (note: Z force equals zero).

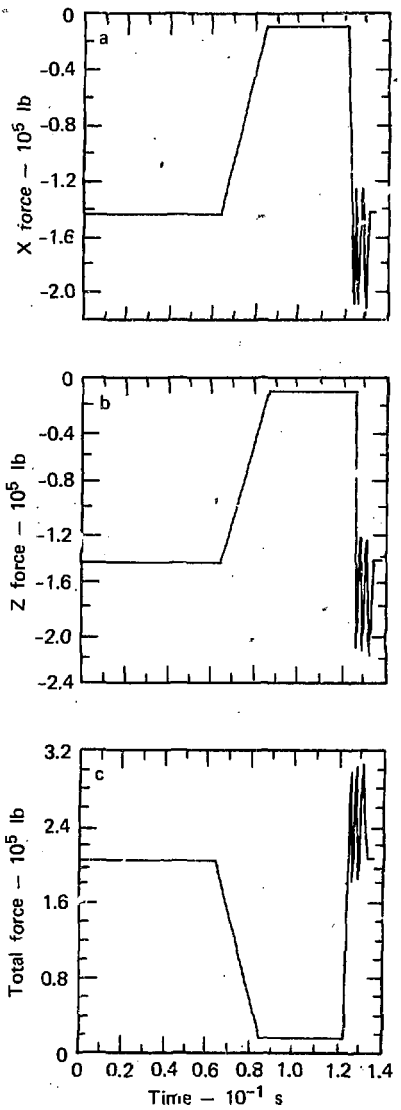

Fig. 23. Case 4 — forces at Junction 16, PTA calculation (note: Y force equals zero).

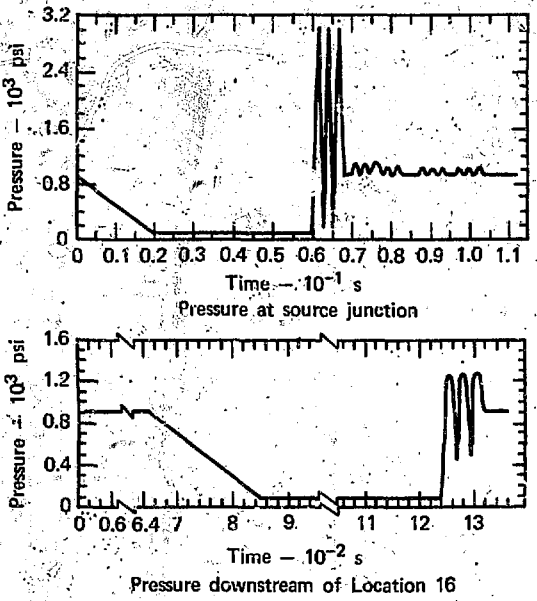

Fig. 24. Case 4 — representative pressure traces, WHAM calculation.

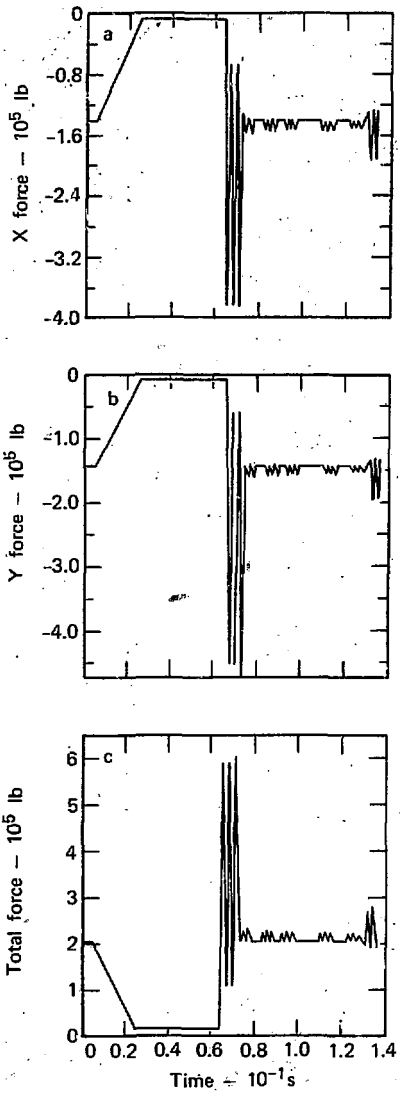

Fig. 25. Case 4 — forces at Junction 1, WHAM calculation (note: Z force equals zero).

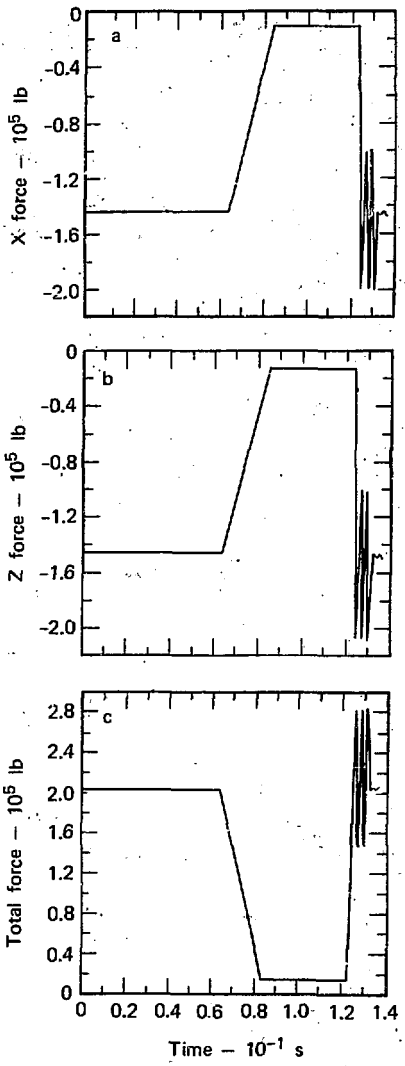

Fig. 26. Case 4 — forces at Junction 16, WHAM calculation (note: Y force equals zero).

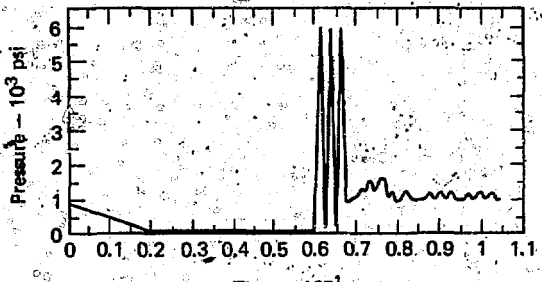

Pressure at source junction

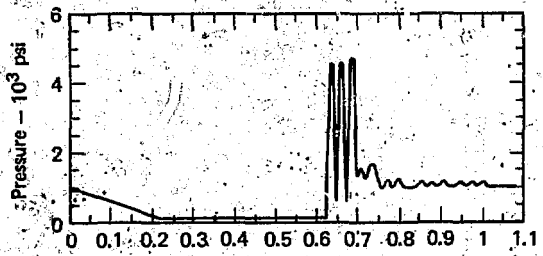

Pressure at location 0

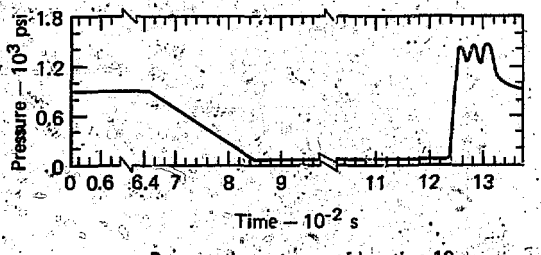

Pressure downstream of location 16

Fig. 27. Case 5 — representative pressure traces.

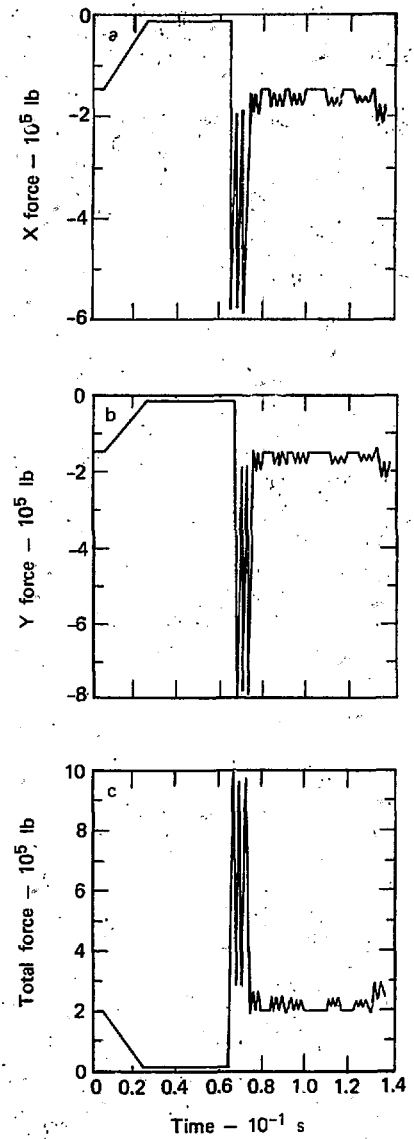

Fig. 28. Case 5 – forces at Junction 1, (note: Z force equals zero).

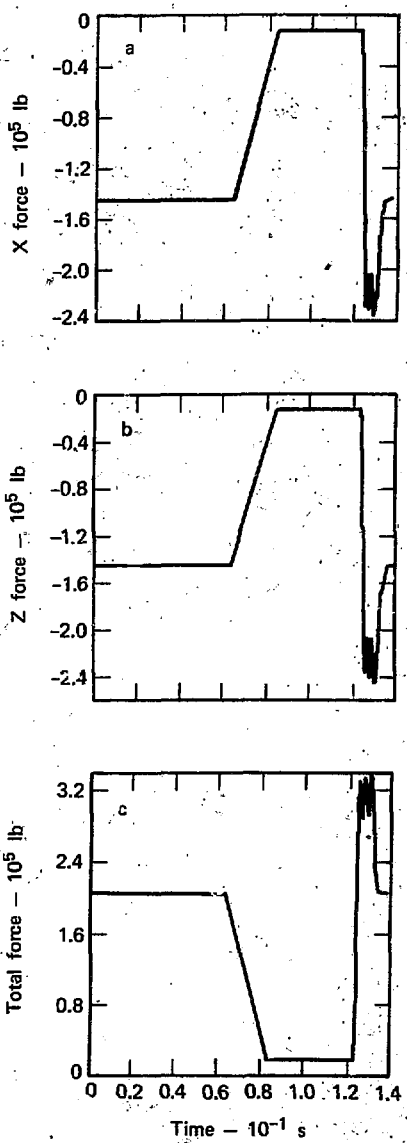

Fig. 29. Case 5 – forces at Junction 16 (note: Y force equals zero).

Section 8
Conclusions

As a result of this study, we have drawn the following conclusions:

- The PTA and WHAM computer codes are both reasonable computational tools to use in this type of analysis, and results from the codes compare favorably.
- Use of an increased lumped friction, several orders of magnitude larger than the steady-state value, appears to be a reasonable method to model elbow and valve losses in dynamic situations.
- Valve and elbow losses can be significant in reducing pressure force and momentum values associated with the spike portions of the pressure pulse. In the cases considered, the peak pressure level going into Location 1 (Fig. 11) was reduced to at least 45% of its value after passing through the 16 loss components of the system.

In addition, we should point out that the importance of including loss mechanisms cannot be fully assessed until the completion of the dynamic structural analysis (Phase II).

Appendix A
Feedwater Line Material and Water Properties at Elevated Temperatures

FEEDWATER LINE MATERIAL PROPERTIES

As mentioned in Table 1 (Section 4), our typical feedwater pipe is made of SA-106, Class C steel. A complete stress-strain curve f this mat rial at elevated temperatures was unavailable. Data that we were able to obtain on the behavior of this material at elevated temperatures are given in Table A-1. In addition, in 1971, personnel at the Lawrence Livermore Laboratory (LLL) performed room temperature tensile tests of SA-106, Class B steel.[32] The stress-strain curve resulting from their test is given in Fig. A-1. Based on these properties, we have constructed an estimate of the stress-strain curve for SA-106, Class C steel at 300°F as shown in Fig. A-2. The ideal representation as used in e PTA calculations is also given.

Table A-1. Property variation of SA106 Class C steel with tempera ure.

	Temperature, °F					
	80	200	300	400	500	600
Elastic modulus (10^6 psi)[30]	29.9	29.5	29.0	28.3	27.4	26.7
Poisson's ratio	0.30	-	-	-	-	-
Yield strength (10^3 psi)[30]	40.	36.5	35.4	34.3	32.3	29.6
(Ref. 31)	42.0	-	38.0	-	34.0	-
Tensile strength (10^3 psi)[31]	72.0	-	80.5	-	75.5	-
Elongation (%)[31]	31.0	-	24.0	-	22.0	-

WATER PROPERTIES

A knowledge of the properties of water at elevated temperatures and pressures is necessary to provide proper input to the computer codes (described in Section 6). Extensive water property data were obtained,[33] and polynomial functions were fit to it. The data for density and sound velocity are shown in Fig. A-3. The data cover a temperature range from 50 to 500°F and a pressure range from 14.7 to 1500 psia. These properties, particularly density, are relatively insensitive to pressure. We are thus justified in neglecting pressure

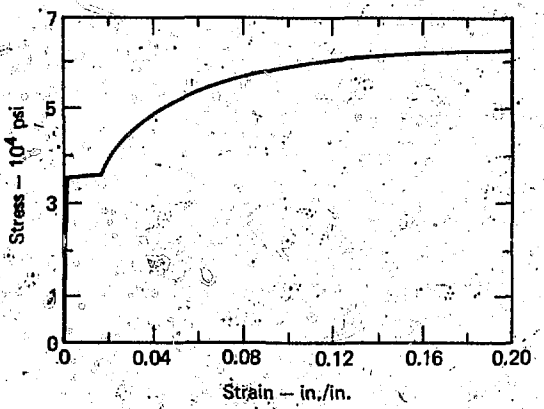

Fig. A-1. Stress-strain curve for SA-106 Class B steel at room temperature.[32]

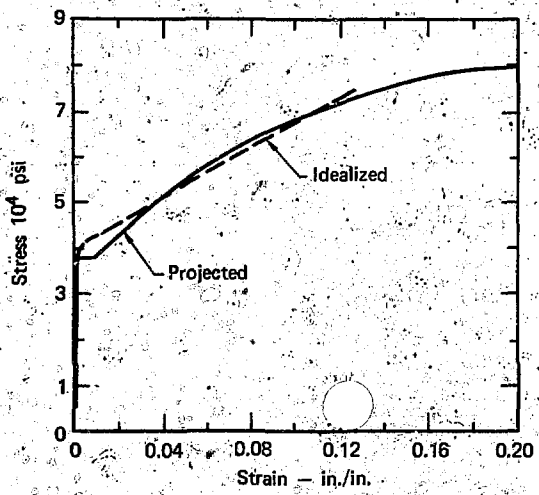

Fig. A-2. Stress-strain curve used in Cases 3 and 5.

effects on the sound speed and density of water. The appropriate polynomial fits are

$$\rho = 62.7724 - 2.58006 \times 10^{-3}\, T - 4.96102 \times 10^{-5}\, T^2 \quad , \quad \text{(A-1)}$$

and

$$C_o = 4.8065 \times 10^3 + 3.22783T - 8.18732 \times 10^{-3}\, T^2 - 5.8709 \times 10^{-10}\, T^3 \quad . \quad \text{(A-2)}$$

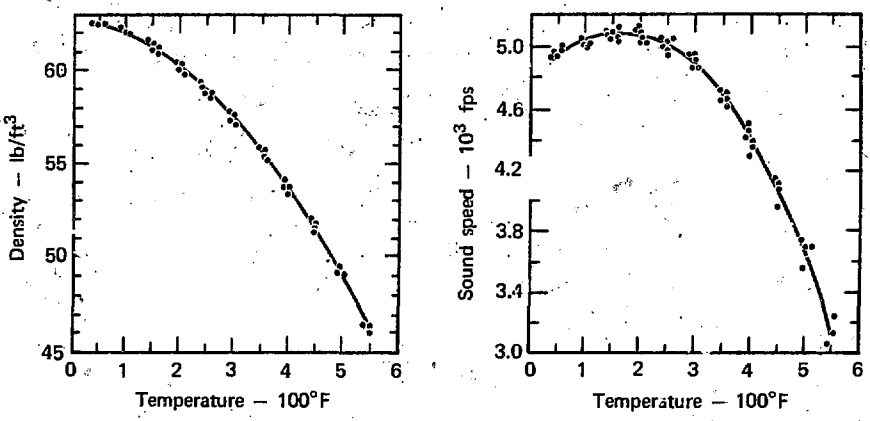

a. Density of water

b. Sound speed of water

Fig. A-3. Water property information.

In these expressions, the temperature (T) is in units of degrees farenheit, density is in units of lbm/ft^3, and sound speed is in units of ft/s.

For viscosity, we have taken the expression[34]

$$\mu \quad [lb\text{-}s/ft^2] \;=\; \frac{1.0225 \times 10^{-3}}{(T-32.)} \qquad (A\text{-}3)$$

In our pressure/temperature region of interest, the error in this simple fit is less than 7% which is sufficiciently accurate for use in the computer calculations.

Appendix B
Summary of PTA and WHAM Solution Methods

PTA SOLUTION METHOD

A brief summary of the solution scheme used in PTA is given below, with further details found in Refs. 12, 14, and 35.

PTA employs the method of characteristics to solve the one-dimensional incompressible flow equations

$$\rho\left(\frac{\partial u}{\partial t} + u\frac{\partial u}{\partial x}\right) + \frac{\partial P}{\partial x} + \frac{f\rho\, u|u|}{2D} = 0 \quad , \tag{5}$$

$$\frac{\partial \rho}{\partial t} + \frac{\partial}{\partial x}(\rho u) = 0 \quad , \tag{B-1}$$

or

$$\frac{\partial \rho}{\partial t} + \rho\frac{\partial u}{\partial x} + u\frac{\partial \rho}{\partial x} = 0 \quad . \tag{B-2}$$

Using the isentropic relation,

$$c^2 = \left(\frac{\partial P}{\partial \rho}\right)_s \quad . \tag{B-3}$$

Equation B-2 becomes

$$\rho c^2\frac{\partial u}{\partial x} + \frac{\partial P}{\partial t} + u\frac{\partial P}{\partial x} = 0 \quad . \tag{6}$$

Equations 5 and 6 are the forms used in PTA. They are of the hyperbolic type for which characteristic solutions exist.

In the theory of the method of characteristics a solution can be defined along a characteristic direction. A linear combination of Eqs. 5 and 6 produces the compatability equations[35]

$$\frac{du}{dt} + \frac{1}{\rho c}\frac{dP}{dt} + \frac{fu|u|}{2D} = 0 \tag{B-4}$$

along the C^+ characteristic

$$dx = (u + c)dt \ , \tag{B-5}$$

and

$$\frac{du}{dt} - \frac{1}{\rho c}\frac{dP}{dt} + \frac{fu|u|}{2D} = 0 \ . \tag{B-6}$$

along the C^- characteristic

$$dx = (u - c)dt \ . \tag{B-7}$$

A combination of Eqs. B-4 and B-6 produces the solution at an adjoining point at the next time step. In finite difference forms we have

$$U_P^{n+1} - U_A^n + \frac{1}{\rho C_A^+}\left(P_P^{n+1} - P_A^n\right) + \frac{f\, U_A^+|U_A^+|\Delta t}{2D} = 0 \ , \tag{B-8}$$

and

$$U_P^{n+1} - U_B^n - \frac{1}{\rho C_B^+}\left(P_P^{n+1} - P_B^n\right) + \frac{f\, U_B|U_B|\Delta t}{2D} = 0 \ , \tag{B-9}$$

which can be solved explicitly for U_P and P_P:

$$U_P^{n+1} = \left[C_A^+\left(U_A^n - g_A\Delta t\right) + C_B^-\left(U_B^n - g_B\Delta t\right) + \left(P_A^n - P_B^n\right)/\rho\right] \Big/ \left(C_A^+ + C_B^-\right), \tag{B-10a}$$

and

$$P_P^{n+1} = \left[P_A/C_A^+ + P_B/C_B^- + \rho\left(U_A^n - g_A\Delta t - U_B^n + g_B\Delta t\right)\right] C_A^+ C_B^- \Big/ \left(C_A^+ + C_B^-\right). \tag{B-10b}$$

Subscripts A and B denote characteristic "waves" starting at locations A and B and converging on location P at the end of the time step. Equations B-10a and B-10b are used at all interior nodes. The alternate forms of these equations used at the junctions of two or more pipes are discussed in Refs. 12 and 14.

WHAM SOLUTION METHOD

A brief summary of the solution method used in the WHAM computer code is given below with further details found in Ref. 15.

WHAM employs the method of wave superposition to solve the one-dimensional incompressible flow equations

$$\rho\left(\frac{\partial u}{\partial t} + u\frac{\partial u}{\partial x}\right) + \frac{\partial P}{\partial x} + \frac{f\rho u|u|}{2D} = \quad (5)$$

and

$$\rho C^2 \frac{\partial u}{\partial x} + \frac{\partial P}{\partial t} + u\frac{\partial P}{\partial x} = 0^* \quad . \quad (6)$$

If we take the density to be constant, we can then say

$$\frac{1}{\rho}\frac{\partial P}{\partial t} = \frac{\partial H}{\partial t} \quad \text{and} \quad \frac{1}{\rho}\frac{\partial P}{\partial x} = \frac{\partial H}{\partial x} \quad . \quad (B\text{-}11)$$

Thus, Eqs. 8 and 9 become

$$\frac{\partial u}{\partial t} + u\frac{\partial u}{\partial x} + \frac{\partial H}{\partial x} + \frac{fu|u|}{2D} = 0 \quad , \quad (B\text{-}12)$$

and

$$C^2 \frac{\partial u}{\partial x} + \frac{\partial H}{\partial t} + u\frac{\partial H}{\partial x} = 0 \quad . \quad (B\text{-}13)$$

The remainder of the solution scheme is attributable to Streeter 9 and Parmakian.[10] Neglecting the friction and convection terms, Eqs. B-12 and B-13 become

$$\frac{\partial u}{\partial t} + \frac{\partial H}{\partial x} = 0 \quad , \quad (B\text{-}14)$$

and

$$C^2 \frac{\partial u}{\partial x} + \frac{\partial H}{\partial t} = 0 \quad , \quad (B\text{-}15)$$

which can be cast into the form

$$\frac{\partial^2 u}{\partial t^2} = C^2 \frac{\partial^2 u}{\partial x^2} \quad , \quad (B\text{-}17)$$

and

$$\frac{\partial^2 H}{\partial t^2} = C^2 \frac{\partial^2 H}{\partial x^2} \quad . \quad (B\text{-}17)$$

---

* The development of Eq. 6 is given in the previous discussion of the PTA solution method.

The solution of these equations represent two waves traveling with the velocity of sound in opposite directions. Thus,

$$u_i^{n+1} - u_o^o = \frac{g}{C}\left(F_i^{n+1} - f_i^{n+1}\right) \quad , \tag{B-18}$$

and

$$p_i^{n+1} - p_o^o = \rho\left(F_i^{n+1} + f_i^{n+1}\right) \quad . \tag{B-19}$$

The wave traveling in the negative x-direction is noted by f while the wave traveling in the positive x-direction is denoted by F.

Since friction is neglected, the wave advances through space unaltered. That is to say:

$$F_i^{n+1} = F_{i-1}^n \quad , \tag{B-20}$$

and

$$f_i^{n+1} = f_{i+1}^n \quad . \tag{B-21}$$

If pipe friction is to be used, the concept of a ficitiious orifice at each internal nodal point is used (Fig. B-1). From Bernoulli's equation, about node i we can say

$$\frac{1}{\rho} p_{i-} + \frac{u_i^2}{2} = \frac{1}{\rho} p_{i+} + \frac{u_i^2}{2} + K_f \frac{u_i^2}{2g} \quad . \tag{B-22}$$

Application of Eqs. B-18 through B-21 in Eq. B-22 provides the quantities u_i^{n+1}, p_i^{n+1} in terms of the old wave values; and the new wave values F^{n+1}, f^{n+1} in terms of old wave values and the new velocity u^{n+1}.

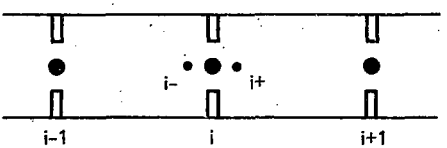

Fig. B-1. Discrete orifice configuration.

Appendix C
Development of the Force Equations Used in PTA and WHAM

The basic equation used to calculate the three force components in an orthogonal 1,2,3, (X,Y,Z) coordinate system is

$$\bar{F}_i = \bar{F}_W \cdot \hat{m}_i = -\iint_{C.S.} P(d\bar{A} \cdot \hat{m}_i) + \iint_{C.S.} (\bar{V} \cdot \hat{m}_i)(\rho V \cdot dA)$$

$$+ \frac{\partial}{\partial t} \iiint_{C.V.} \rho(\bar{V} \cdot \hat{m}_i) dv \qquad i = 1,2,3 \tag{9}$$

We evaluate forces at midtime step. That is to say, Eq. 12 can be rewritten as

$$\bar{F}_i^{n+1/2} = \bar{F}_W^{n+1/2} \cdot \hat{m}_i = -\iint_{C.S.} \frac{(P^{n+1} + P^n)}{2} (d\bar{A} \cdot \hat{m}_i)$$

$$+ \rho \iint_{C.S.} \left[\frac{(\bar{V}^{n+1} + \bar{V}^n)}{2} \cdot \hat{m}_i\right] \left[\frac{(\bar{V}^{n+1} + \bar{V}^n)}{2} \cdot d\bar{A}\right]$$

$$+ \frac{\rho}{\Delta t} \iiint_{C.V.} (\bar{V}^{n+1} - \bar{V}^n) \cdot \hat{m}_i \, dv \quad . \tag{C-1}$$

In our study we consider two types of force elements: curved pipe segment (elbow) and straight pipe segment (valves, restrictors, etc.). Details on the application of Eq. C-1 to each of these elements are now given below.

ELBOW SEGMENT

Details of an elbow segment are given in Fig. C-1. Shown is an elbow of angle θ, radius of curvature R, and pipe radius r. Each of the large "dots"

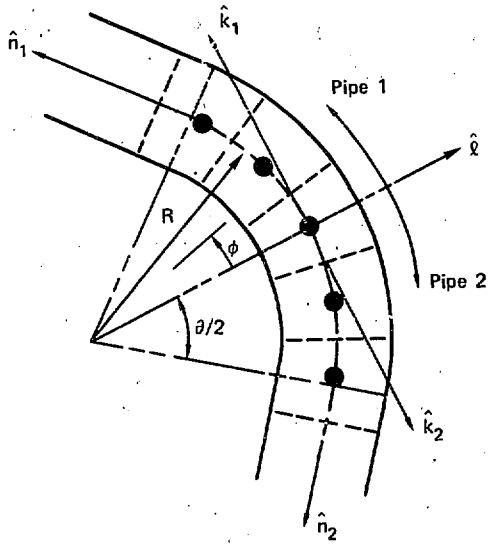

Fig. C-1. Elbow configuration.

represents a nodal point in the calculation, and the dotted lines represent boundaries of control volumes that surround the nodes.

For our analysis we assume, as in PTA and WHAM, that the flow is one-dimensional. That is to say, variations in velocity and pressure exist only in the axial direction. There is none across the pipe cross section. Thus, it is easier to write all velocity and pressure components within the elbow in terms of the three unit vectors k_1, k_2, and ℓ where we define

$$\hat{\ell} = \frac{(\hat{n}_1 + \hat{n}_2)/2}{|(\hat{n}_1 + \hat{n}_2)/2|}, \qquad \text{(C-2a)}$$

and

$$\hat{k}_1 = \frac{(\hat{\ell} \times \hat{n}_1) \times \hat{\ell}}{|(\hat{\ell} \times \hat{n}_1) \times \hat{\ell}|} . \qquad \text{(C-2b)}$$

Note that k_1, and k_2 as defined in Eq. C-2b are unit vectors and that $k_2 = -k_1$. From Fig. C-1, we can see that for pipe 1, the velocity at any given angle ϕ (measured from the vector ℓ) is given by

$$\overline{V}_i = -(V_1 \sin\phi)\,\hat{\ell} + (V_1 \cos\phi)\,\hat{k}_1 \quad . \tag{C-3a}$$

Likewise, for pipe 2:

$$\overline{V}_2 = -(V_2 \sin\phi)\,\hat{\ell} + (V_2 \cos\phi)\,\hat{k}_2 \quad , \tag{C-3b}$$

where V_1 represents the magnitude of the velocity along the axis of pipe 1 (in the n_1 direction) and V_2 represents the magnitude of the velocity along the axis of pipe 1 (in the n_2 direction).

Thus, keeping in mind that the flow is one-dimensional, we have from Eq. C-1,

$$\overline{F}_i = -\sum_j \frac{(P^{n+1} - P^n)}{2} A_j\,(\hat{n}_j \cdot \hat{m}_1) + \rho \sum_j \left[\frac{V^{n+1} + V^n}{2}\right]^2 (\hat{n}_j \cdot \hat{m}_j)$$

$$+ \frac{\rho AR}{\Delta t}\left\{\int_0^{\Theta/2}\left[-\left(V_1^{n+1} - V_1^n\right)\sin\phi\,(\hat{\ell}\cdot\hat{m}_1) + \left(V_1^{n+1} - V_1^n\right)\cos\phi\,(\hat{m}_i \cdot \hat{k}_1)\right] d\phi_1\right.$$

$$\left. + \int_0^{\Theta/2}\left[-\left(V_2^{n+1} - V_2^n\right)\sin\phi\,(\hat{\ell}\cdot\hat{m}_1) + \left(V_2^{n+1} - V_2^n\right)\cos\phi\,(\hat{m}_i \cdot \hat{k}_2)\right] d\phi_2\right\} . \tag{C-4}$$

Within each control volume, we assume a linear variation in velocity. Referring to Fig. C-2, we have between ϕ_{k-1} and ϕ_k:

$$V = V_k + \left(\frac{V_k - V_{k-1}}{\phi_k - \phi_{k-1}}\right)(\phi - \phi_k); \tag{C-5a}$$

likewise, between ϕ_k and ϕ_{k+1}:

$$V = V_k + \left(\frac{V_{k+1} - V_k}{\phi_{k+1} - \phi_k}\right)(\phi - \phi_k) \quad . \tag{C-5b}$$

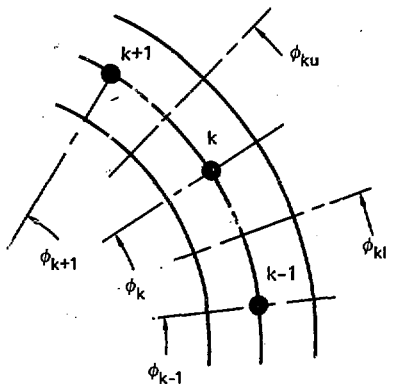

Fig. C-2. Elbow nodal point control volume nomenclature.

For example, if we apply these rations to one of the integral terms in Eq. C-4, for a single control volume as shown in Fig. C-2:

$$\int_{\phi_{kl}}^{\phi_k} \left(V_1^{n+1} - V_1^n\right) \cos\phi\ (\hat{m}_i \cdot \hat{k}_1)\, d\phi_1 = (\hat{m}_i \cdot \hat{k}_i)\left\{\left[\left(V_k^{n+1} - V_k^n\right) - \phi_k\left(dV_{kl}^{n+1} - dV_{kl}^n\right)\right](\mathrm{Sin}\phi_k - \mathrm{Sin}\phi_{kl}) + \left(dV_{kl}^{n+1} - dV_{kl}^n\right)(\cos\phi_k - \cos\phi_{kl} + \phi_k \sin\phi_k - \phi_{kl}\sin\phi_{kl})\right\}, \qquad \text{(C-6a)}$$

and

$$\int_{\phi_k}^{\phi_{ku}} \left(V_1^{n+1} - V_1^n\right) \cos\phi\ (\hat{m}_i \cdot \hat{k}_1)\, d\phi_1 = (\hat{m}_i \cdot \hat{k}_1)\left\{\left[\left(V_k^{n+1} - V_k^n\right) - \phi_k\left(dV_{ku}^{n+i} - dV_{ku}^n\right)\right](\mathrm{Sin}\phi_{ku} - \mathrm{Sin}\phi_k) + \left(dV_{ku}^{n+1} - dV_{ku}^n\right)(\cos\phi_{ku} - \cos\phi_k + \phi_{ku}\sin\phi_{ku} - \phi_k \sin\phi_k)\right\}, \qquad \text{(C-6b)}$$

where

$$dV_{kl}^{n} = \frac{V_k^n - V_{k-1}^n}{\phi_k - \phi_{k-1}} \quad , \quad dV_{ku}^{n} \frac{V_{k+1}^n - V_k^n}{\phi_{k+1} - \phi_k} \quad . \tag{C-7}$$

Similar expressions are derivable for the other components.

STRAIGHT PIPE SEGMENT

As shown in Figure C-3, we consider a straight pipe force segment to consist of three nodal points and their surrounding control volumes.

Equation C-1 thus takes the form,

$$\overline{F}_i^{n+1/2} = \overline{F}_W^{n+1/2} \cdot \hat{m}_i = -\sum_j \frac{(P^{n+1} + P^n)}{2} A_j (\hat{n}_j \cdot \hat{m}_i)$$

$$\rho \sum_j \left[\frac{V^{n+1} - V^n}{2}\right]^2 (\hat{n}_j \cdot \hat{m}_i) + \frac{\rho A}{\Delta t} \int_0^{\ell_1} (V_1^{n+1} - V_1^n)(\hat{n}_1 \cdot \hat{m}_i)\, dX$$

$$+ \frac{\rho A}{\Delta t} \int_0^{\ell_2} (V_2^{n+1} - V_2^n)(\hat{n}_2 \cdot \hat{m}_i)\, dX \quad . \tag{C-8}$$

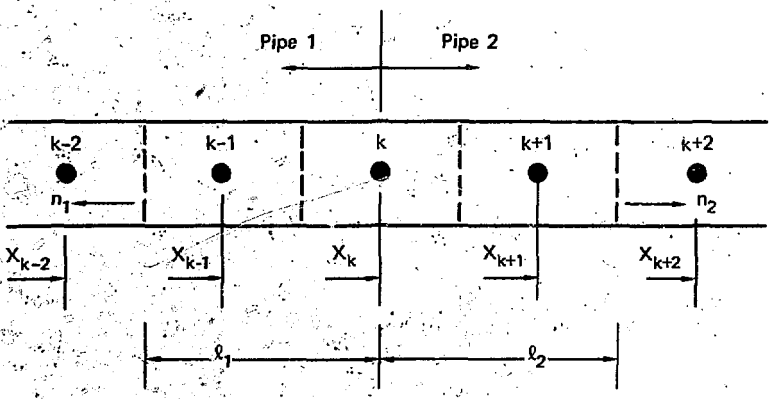

Fig. C-3. Straight pipe segment configuration.

As with the elbow element, we assume a linear velocity variation. Thus, between X_{k-1} and X_k:

$$V = V_k + \left(\frac{V_k - V_{k-1}}{X_k - X_{k-1}}\right)(X - X_k) \quad . \tag{C-9}$$

Similarly, between X_k and X_{k+1}:

$$V = V_k + \left(\frac{V_{k+1} - V_k}{X_{k+1} - X_k}\right)(X - X_k) \quad . \tag{C-10}$$

Applying these relations to one of the integrals in Eq. C-8, we have for example,

$$\frac{\rho A}{\Delta T}\int_0^{\ell_1}\left(V_1^{n+1} - V_1^n\right)(\hat{n}_1 \cdot \hat{m}_1)\, dX = \frac{\rho A}{\Delta t}\left[\left(\frac{V_k + 2V_{k-1} + V_{k-2}}{2}\right)^{n+1} - \left(\frac{V_k + 2V_{k-1} + V_{k-2}}{2}\right)^{n}\right] \cdot |X_k - X_{k-1}|\,(\hat{n}_1 \cdot \hat{m}_i) \quad . \tag{C-11}$$

Appendix D
Code Verification Calculation Details

To verify the calculational correctness of the LLL versions of PTA and WHAM, we performed a series of benchmark calculations. Included are problems to test the basic computational scheme, elbow loss modeling, and the plasticity modeling in PTA.

BASIC COMPUTATIONAL METHOD TEST PROBLEMS

The geometries for the first set of problems, which we will denote as test problems T1.1 and T1.2, are given in Fig. D-1. These problems model the situation of uniform flow in a pipe in the presence of an instantaneously closing valve. In our calculation we model the very rapid valve closure by having the flow impact against a rigid end wall. Problem T1.1 is the rigid wall case, and problem T1.2 is the flexible or elastic pipe case. We selected these problems since they have simple analytical solutions. As discussed by Streeter,[9] the magnitude of the step-type pressure wave that propagates back into the fluid from the rigid end is given by

$$P - P_o = \rho_o C_w |V_o| \quad . \tag{D-1}$$

The wave propagation velocity[9,12,14,24] is given by

$$\text{Rigid wall: } C_w = C_o \text{ (fluid sonic velocity)} \tag{D-2a}$$

$$\text{Flexible Wall: } C_w = C_E \text{ (elastic wave velocity)} = \left(\frac{1}{C_o^2} + \frac{D\rho}{EH}\right)^{-1/2} \tag{D-2b}$$

For these problems we took the initial pressure (P_o) to be 14.5 psia, the initial velocity (V_o) to be 60.4 fps, the water density (ρ) to be 62.4 lbm/ft^3, and the speed of sound in water (C_o) to be 4990 fps. In the flexible wall problem, the pipe outside diameter (D) was 2.61 in., and the pipe wall thickness (H) was 0.13 in. The material properties used for the pipe wall in test problem T1.2 are given in Table D-1. The detailed material properties given in Table D-1 are not required for the simple PTA and WHAM calculations.

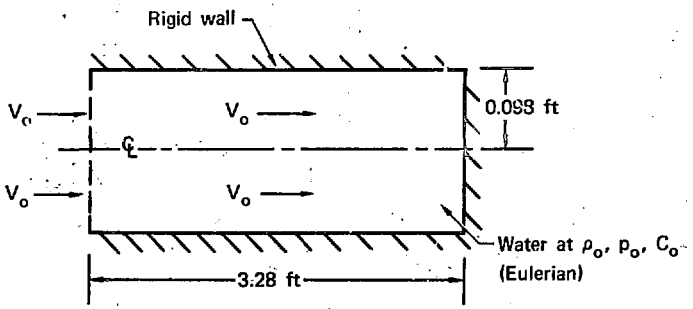

Problem T1.1 – Rigid wall

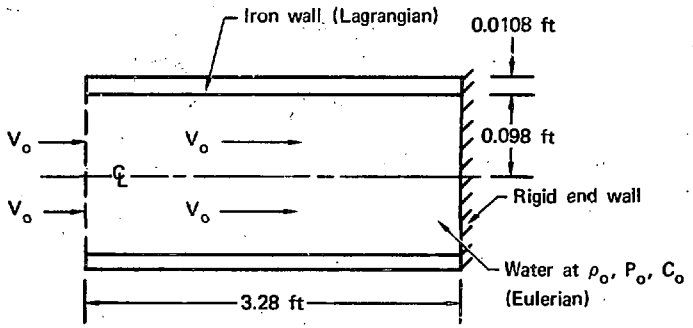

Problem T1.2 – Flexible wall

Fig. D-1. Geometries for test problems T1.1 and T1.2.

Table D-1. Pipe material properties for Problem T1.2.

Density	486.5 lb/ft^3
Bulk Modulus	27.3 × 10^6 psi
Shear Modulus	11.3 × 10^6 psi
Elastic modulus	29.8 × 10^6 psi
Poisson ratio	0.32
Yield strength	Infinite

To investigate the effect of radial pipe motion on the flow, we also calculated this problem by using the CHAMP computer code,[36-38] which requires detailed pipe material properties. CHAMP is an LLL-developed Eulerian/Lagrangian coupled code. It treats the fluid in the Eulerian frame and the structure (pipe wall) motion in the Lagrangian frame. Results of these calculations are given in Figs. D-2 and D-3. In Fig. D-2, results for the rigid wall problem T1.1 are shown. With respect to pressure magnitude, the PTA and WHAM calculations compare to within 0.1% of the theoretical 4070-psi pressure jump obtained from Eqs. D-1 and D-2a. The CHAMP calculation is within 4% of the theoretical prediction. The WHAM calculation exhibits a very sharp front, characteristic of the wave superposition solution method. The PTA calculation exhibits a slightly more gradual rise, which is a result of a slight amount of numerical dispersion in the solution approach. The CHAMP calculation exhibits an even more gradual rise because of the artificial viscosity in the solution scheme which, for numerical purposes, smears the shock front over several cells. Results for the flexible elastic wall problem is given in Fig. D-3. Again, with respect to pressure magnitude, the PTA and WHAM calculations compare to within 0.1% of the theoretical 3878-psi pressure jump obtained from Eqs. D-1

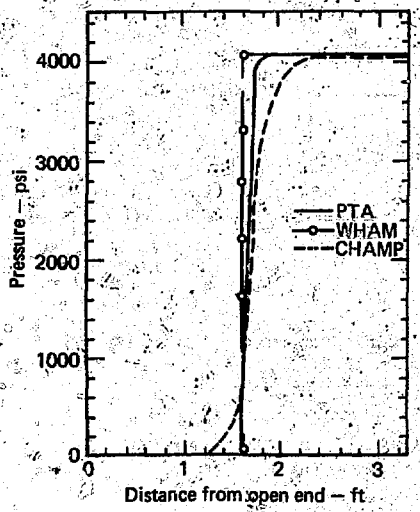

Fig. D-2. PTA, WHAM and CHAMP results for test problem T1.1 at 320 μs.

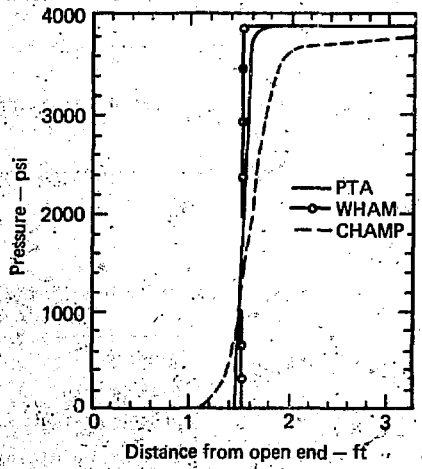

Fig. D-3. PTA, WHAM and CHAMP results for test problems T1.2 at 375 μs.

and D-2b. Note how the pressure wave in the CHAMP calculation has an increasing tail. At the time plotted, the maximum pressure is still well below the theoretical value because of pipe wall oscillation. Figure D-4 is a plot of inner boundary radial displacement near the end wall. Note how the motion appears to oscillate. As this motion damps out, the pressure at that location rises to within 3% of the theoretical value.

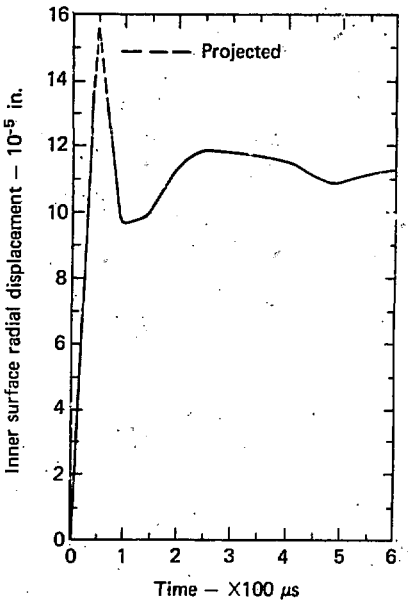

Fig. D-4. Time history of radial displacement at the inner boundary (representative).

ELBOW LOSS TEST PROBLEM

To verify the elbow loss model discussed in Section 6 we calculated the elbow loss experiment conducted by Romander.[22] Figure D-5 describes the experiment configuration, including the relationship of the elbow to the pulse gun. By the time the pulse reaches the elbow, yielding of the flexible pipe has reduced the pulse magnitude to the yield point. Thus, reduction in the pulse magnitude as it transits the elbow is caused either by the impedence

discontinuity* or "viscous" losses. In this instance, the discontinuity is caused by both material-property and wall-thickness differences. The pipe inside diameter is 2.85 in. The flexible pipe has an elastic modulus of 27×10^6 psi and a wall thickness of 0.040 in. For water at 70°F, the sonic velocity is 4990 fps. Thus, from Eq. D-2 the flexible pipe has an elastic wave velocity of 3979 fps while the rigid pipe (elbow) has a wave velocity of 4990 fps. The experimental pressure trace at Location 1 is shown in Fig. D-6. The dashed line is the idealization used as a boundary condition in the calculations.

The first of this set of problems, which we shall denote as problem T2.1, is a demonstration of the effect of the impedence discontinuities. The predicted trace at Location 2 along with the experimental trace at Location 2 are given in Fig. D-7. Note that the impedence discontinuity causes little loss. In PTA, however, it produces a "shewing" of the pulse peak. Results for problem T2.2 are given in Fig. D-8. In this instance we have added a lumped friction of

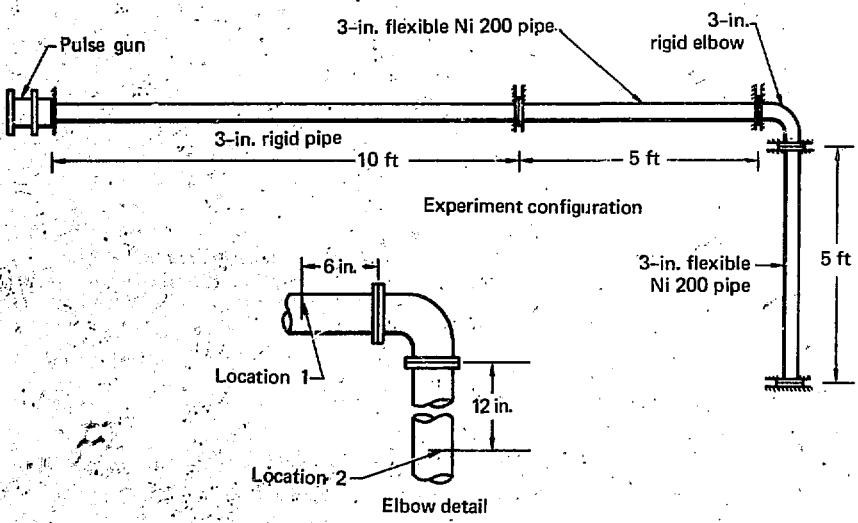

Fig. D-5. Geometry in Romander experiments.[22]

*An impedence discontinuity exists where there is a discontinuous change in the wave velocity. For example, it results at the junction of two pipes of either different elastic and plastic properties, area (diameter) or wall thickness.

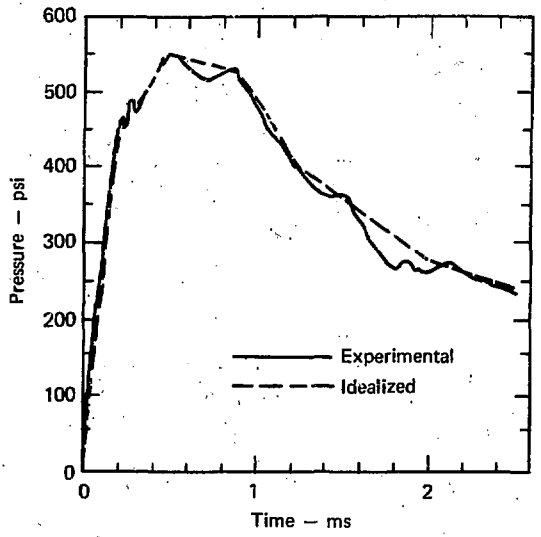

Fig. D-6. Pressure pulse at Location 1 (Fig. D-5).

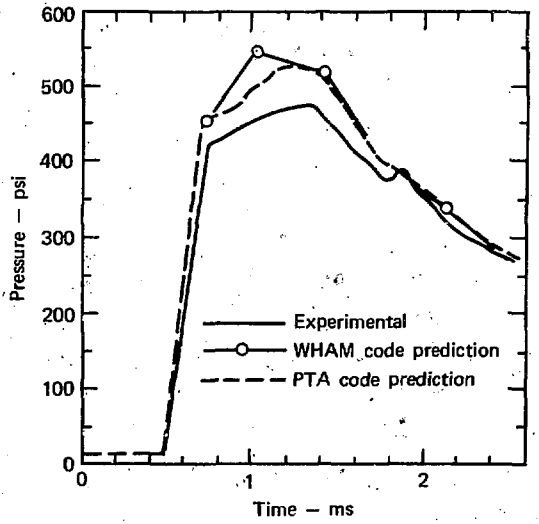

Fig. D-7. Effect of impedance discontinuity on pressure pulse — pressure at Location 2.

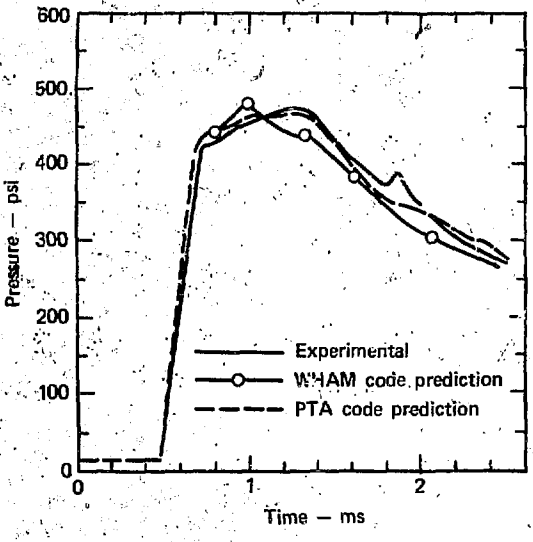

Fig. D-8. Elbow loss calculation results — pressure at Location 2.

1.5×10^4 to the calculation. This factor is approximately three orders of magnitude greater than steady-state loss factors for a 90° elbow. Note that the comparison between the experimental trace and the numerical prediction is remarkably good. The serves to demonstrate the usefulness of an increased lumped friction factor in modeling elbow losses.

PTA PLASTICITY TEST PROBLEM

Since we selected initial pulse magnitudes that are sufficient to cause yielding of the pipe, we performed a test calculation Problem T3 to verify the plasticity model in the PTA computer code. This problem is an independent calculation of the problem discussed by Youngdahl and Kot,[12] which is from the experimental results of Florence and Abrahamson.[20] The experimental configuration is given in Fig. D-9. The stress strain curve for the pipe material is shown in Fig. D-10. The idealized input pulse, applied at Location 1, is shown in Fig. D-11. Comparisons of the experimental and numerically predicted pressure pulses at Location 2 is shown in Fig. D-12. Our calculation reproduces the results given by Youngdahl and Kot.[12]

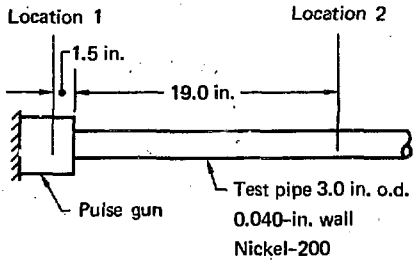

Fig. D-9. Plasticity test-problem configuration.

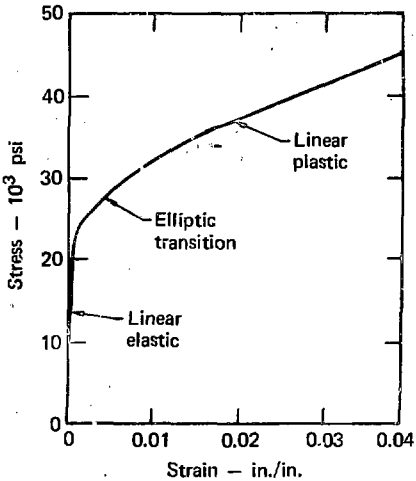

Fig. D-10. Pipe stress-strain curve for problem T3.

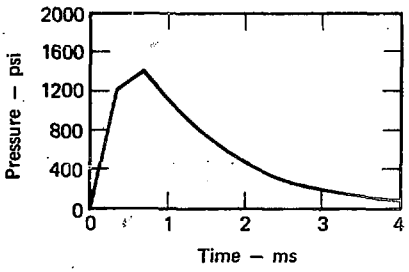

Fig. D-11. Plasticity test-problem input pulse.

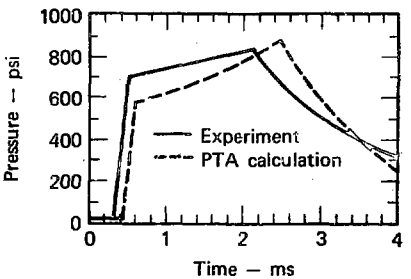

Fig. D-12. Pressure traces at Location 2.

References

1. J. A. Block et al., *An Evaluation of PWR Steam Generator Water Hammer*, Creare Incorporated, Hanover, N.H., NUREG-0291 (June 1977).
2. Consolidated Edison Co., *Indian Point Station, Unit 2. Feedwater Line Incident Report*, New York City, N.Y., Docket-50247-191 (January 14, 1974).
3. R. T. Carlson (NRC) and A. E. Lundvall, Baltimore Gas and Electric Company, private communication (May 28, 1975), Docket 50-317.
4. F. J. Tokarz, Lawrence Livermore Laboratory, and V. Stello, NRC/DOR discussing NRC/DOR project status, private communication (March 14, 1977).
5. J. A. Vreeland, "Evidence of Very Large Condensation Rates at High Pressure," *16th National Heat Transfer Conference, St. Louis, Missouri (August 8-11, 1976)*.
6. Consolidated Edison Co., *Indian Point Station, Unit 2: Results of Test Program Following Plant Revisions Affecting Feedwater Piping*, Docket-50247-219 (March 12, 1974).
7. K. Jabbour (NRC/DOR) and D. Arthur (Lawrence Livermore Laboratory), private communication (November 1976).
8. D. Batchelor, T. Cecchi, and V. Shoa, "Analysis of Tihange Main Feedwater Lines Behavior During a Water Hammer Event," *Foratom*, Madrid, Spain (1976.)
9. V. L. Streeter, *Hydraulic Transients* (McGraw-Hill Book Co., New York, N.Y., 1955).
10. J. Parmakian, *Water Hammer Analysis* (Prentice-Hall, Inc., New York N.Y., 1955).
11. W. T. Rouleau, "Pressure Surges in Pipelines Containing Viscous Liquids," *ASME, Journal of Basic Engineering*, pp. 912-920 (Dec. 1960).
12. C. Youngdahl and C. Kot, "Effect of Plastic Deformation of Piping on Fluid-Transient Propagation," *Nuclear Eng. and Design*, 35 (1975).
13. V. L. Streeter and L. Chintu, "Water Hammer Analysis Including Fluid Friction," *ASCE Proc. Paper 3135* (May 1962).
14. C. K. Youngdahl and C. A. Kot, *PTA-1, A Computer Program for Analysis of Pressure Transients in Hydraulic Networks Including the Effect of Pipe Plasticity*, Argonne National Laboratory, Argonne, Illinois, ANL-76-64 (1976).

15. S. Fabic, "Computer Program WHAM for Calculation of Pressure, Velocity, and Force Transients in Liquid Filled Piping Networks," Kaiser Engineers, Report 67-49-R (1967).

16. I. Shames, *Mechanics of Fluids* (McGraw-Hill Book Company, New York, 1962).

17. D. Stephenson, "Water Hammer Charts Including Fluid Friction," *ASCE, Journal of Hydraulics Division,* pp. 71-94 (September 1966).

18. P. Lieberman and E. Brown, "Pressure Oscillations in a Water-Cooled Nuclear Reactor Induced by Water Hammer Waves," *ASME, Journal of Basic Engineering,* pp. 901-911 (Dec. 1960).

19. W. Zielke, "Frequency - Dependent Friction in Transient Pipe Flow," *ASME, Journal of Basic Engineering,* pp. 109-115 (March 1968).

20. A. L. Florence and G. R. Abrahamson, "*Simulation of a Hypothetical Core Disruptive Accident in a Fast Flux Test Facility,* Stanford Research Institute, Menlo Park, Calif., HEDL-SRI-1 (May 1973).

21. A. L. Florenze, "Pulse Propagation in Fluid-Filled Pipes," *Third Int. Conf. on Structural Mechanics in Reactor Technology,* (London, England, 1976) vol. 2, Part F, paper F4/8.

22. C. M. Romander, et al., *Experiments on the Response of Flexible Piping Systems to Internal Pressure Pulses,* Stanford Research Institute, Menlo Park, Calif., PYD-1960 (April 1976).

23. Y. W. Chang et al., "Response of the Primary Piping Loop to an HCDA," *Third Int. Conf. on Structural Mechanics in Reactor Technology, London, 1-5 Sept. 1975* (London, England 1975), vol 2, Part F, paper F4/7.

24. G. L. Fox and D. D. Stepnewski, "Pressure Wave Transmission in a Fluid Contained in a Plastically Deforming Pipe," *ASME, Journal of Pressure Vessel Technology,* 262 pp. 258 (Nov. 1974).

25. J. A. Swaffield, "The Influence of Bends on Fluid Transients Propagated in Incompressible Pipe Flow," *Proc. Instn. Mech. Engrs. 1968-69,* vol 183, Pt 1, No. 29, pp. 603-614.

26. D. N. Contractor, "The Reflection of Water Hammer Waves from Minor Losses," *ASME, Journal of Basic Engineering,* pp. 445-452 (June 1965).

27. L. C. Chang and S. R. Johnson, "Blowdown Analysis with Effects of Elbows and Varied Flow Area," *Trans. Am. Nucl. Soc.,* 22 pp. 275-276 (Nov 1975).

28. Crane Co., *Engineering Data Catalog,* VC-1900, New York (1976).

29. K. Jabbour (NRC/DOR) and Dom DiIanni (NRC/DOR) to D. Arthur (Lawrence Livermore Laboratory), private communication (March, 1977).

30. *ASME Boiler and Pressure Vessel Code, Section VIII, Division 2,* American Society of Mechanical Engineers, New York (1971).

31. *Steels for Elevated Temperature Service,* United States Steel Corporation, Pittsburgh, Penn., Data Book ADUSS43-1089-05 (1974).

32. Bob Brady and S. Sutton, Lawrence Livermore Laboratory, private communication (December 1976).

33. V. Berta (Idaho Nuclear Energy Laboratory)and D. Arthur (Lawrence Livermore Laboratory), private communication (October 1976).

34. F. A. Morrison, *Transient Multiphase Multicomponent Flow in Porous Media,* Lawrence Livermore Laboratory, Rept UCRL-51302, (January 1973).

35. Y. Shin, and W. Chen, "Numerical Fluid-Hammer Analysis by Method of Characteristics in Complex Piping Networks, *Nuclear Eng. and Design,* 33, pp. 357-369 (1975).

36. L. Edwards et al., *CHAMP Users Manual,* Lawrence Livermore Laboratory, In preparation.

37. E. D. Groux, *HEMP Users Manual,* Lawrence Livermore Laboratory, Rept. UCRL-51079, Rev. 1 (December 1973).

38. M. L. Wilkins, *Calculation of Elastic-Plastic Flow,* Lawrence Livermore Laboratory, Rept. UCRL-7322, Rev. 1 (1969).

LRS/cld/lc